AD-A241 555
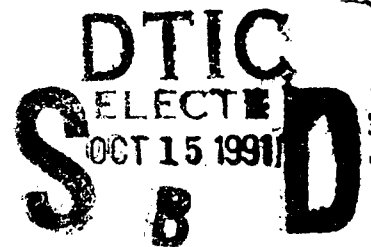
TECHNICAL REPORT BRL-TR-3255

BRL

VARIOUS TARGET MATERIAL FAILURE MECHANISMS OBSERVED FOR BALLISTIC PENETRATIONS

TIMOTHY G. FARRAND

DTIC
ELECTE
OCT 15 1991
S B D

AUGUST 1991

U.S. ARMY LABORATORY COMMAND

BALLISTIC RESEARCH LABORATORY
ABERDEEN PROVING GROUND, MARYLAND

NOTICES

REPORT DOCUMENTATION PAGE	Form Approved OMB No 0704-0188

Public reporting burden for this collection of information is estimated to average 1 hour per response, including the time for reviewing instructions, searching existing data sources, gathering and maintaining the data needed, and completing and reviewing the collection of information. Send comments regarding this burden estimate or any other aspect of this collection of information, including suggestions for reducing this burden, to Washington Headquarters Services, Directorate for Information Operations and Reports, 1215 Jefferson Davis Highway, Suite 1204, Arlington, VA 22202-4302, and to the Office of Management and Budget, Paperwork Reduction Project (0704-0188), Washington, DC 20503

1. AGENCY USE ONLY (Leave blank)	2. REPORT DATE August 1991	3. REPORT TYPE AND DATES COVERED Final, Jun 90 - Feb 91

4. TITLE AND SUBTITLE	5. FUNDING NUMBERS
Various Target Material Failure Mechanisms Observed for Ballistic Penetrations	PR: 1L162618AH80

6. AUTHOR(S)

Timothy G. Farrand

7. PERFORMING ORGANIZATION NAME(S) AND ADDRESS(ES)	8. PERFORMING ORGANIZATION REPORT NUMBER
U.S. Army Ballistic Research Laboratory ATTN: SLCBR-TB-P Aberdeen Proving Ground, MD 21005-5066	

9. SPONSORING MONITORING AGENCY NAME(S) AND ADDRESS(ES)	10. SPONSORING MONITORING AGENCY REPORT NUMBER
U.S. Army Ballistic Research Laboratory ATTN: SLCBR-DD-T Aberdeen Proving Ground, MD 21005-5066	BRL-TR-3255

11. SUPPLEMENTARY NOTES

12a. DISTRIBUTION AVAILABILITY STATEMENT	12b. DISTRIBUTION CODE
Approved for public release; distribution is unlimited.	

13. ABSTRACT (Maximum 200 words)

The failure mechanism of a novel target material is compared to existing armor materials (rolled homogeneous armor, RHA, and high hardness armor, HHA), which exhibit two vastly different failure mechanisms. The RHA steel exhibits large bulk plastic deformation as the penetrator burrows into the target. In contrast, the HHA deforms much less as the strain is localized in very small regions that develop into adiabatic shear bands which "chip" undeformed target material loose during the penetration. Pyromet 718, a nickel superalloy, was chosen to compare different failure mechanisms to the resistance to penetration of the RHA and HHA material. However, it deformed in a manner combining the other two extremes, exhibiting some bulk plastic deformation prior to localizing in deformation bands. The ballistic resistance also appears to lie between the two existing materials with respect to hardness and perhaps, somewhat better for its strength.

14. SUBJECT TERMS		15. NUMBER OF PAGES 64
Adiabatic shear, bulk plastic deformation, deformation, penetration, shear bands, kinetic energy, penetration channel.		16. PRICE CODE

17. SECURITY CLASSIFICATION OF REPORT	18. SECURITY CLASSIFICATION OF THIS PAGE	19. SECURITY CLASSIFICATION OF ABSTRACT	20. LIMITATION OF ABSTRACT
UNCLASSIFIED	UNCLASSIFIED	UNCLASSIFIED	SAR

NSN 7540-01-280-5500

Standard Form 298 (Rev 2-89)
Prescribed by ANSI Std Z39-18
298-102

INTENTIONALLY LEFT BLANK.

TABLE OF CONTENTS

INTENTIONALLY LEFT BLANK.

LIST OF FIGURES

LIST OF TABLES

INTENTIONALLY LEFT BLANK.

ACKNOWLEDGMENTS

INTENTIONALLY LEFT BLANK.

1. INTRODUCTION

The localization of plastic deformation of a material by adiabatic shear banding occurs under high strain rate loading conditions such as high rate machining, upset forging, explosively bursting shells, and terminal ballistic rod-plate penetration. The study of adiabatic shear has been pursued since the initial discovery by Zener and Holloman (1944). Adiabatic shear occurs when a material strain-softens due to a local temperature rise quicker than it work hardens. The highly localized plastic flow behavior, attributed to adiabatic shear banding, is quite different than the typical bulk plastic deformation a material will exhibit if a localization does not develop. When a localized adiabatic shear band is formed, the material within the band is highly deformed to extremely high strains, whereas the material away from the localization is virtually undeformed. In widespread bulk plastic deformation, the entire specimen is plastically deformed to varying degrees throughout the specimen.

This report studies the influence of the susceptibility of various armors to adiabatic shear banding and its resistance to penetration by an impacting projectile. When a projectile is fired into an armor at ordnance (typical tank ammunition) velocities, both the projectile and the target deform as the projectile penetrates into the armor. The manner in which they plastically deform is of considerable interest to the ballistic community. Magness and Farrand (1990) have demonstrated how the deformation mechanism of the penetrator influences its ability to penetrate into an armor.

2. BACKGROUND

2.1 Adiabatic Shear. An adiabatic shear instability can occur when the change in stress with respect to temperature overcomes the normal strain hardening of a material. Thermal softening (a strain-softening behavior) will occur if the material softens due to the local temperature rise quicker than the typical strengthening of the material during plastic deformation. In contrast, during work hardening (i.e., a standard tensile test), the localized area is worked and strain hardened (strengthened), and the subsequent deformation or strain is relocated to another region of the specimen, in turn, increasing the overall strength of the material. For strain softening, an isolated area in the form of a band will develop and will become softer than the surrounding material. All further deformation will be focussed into

1

these localized bands without redistributing the strain to the less worked areas. The localizations tend to occur along planes of maximum shear stress and appear as classic adiabatic shear bands (Zener and Holloman 1944). In theory, the rate of work hardening is locally exceeded by the rate of thermal softening which leads to an instability and a concentration of deformation in a narrow softened band (Flockhart, Woodward, and O'Donnell 1990). The relation between the work hardening, the strain-rate hardening, and the thermal softening can be represented by the following equation by Staker (1981):

$$d\tau = \frac{\partial \tau}{\partial \gamma})_{T,\dot{\gamma}} d\gamma \; + \; \frac{\partial \tau}{\partial T})_{\gamma,\dot{\gamma}} dT \; + \; \frac{\partial \tau}{\partial \dot{\gamma}})_{T,\gamma} d\dot{\gamma} \tag{1}$$

| Work Hardening [1] | Thermal Softening [2] | Strain-Rate Sensitivity [3] |

where,

τ = shear stress,

γ = shear strain,

T = temperature,

and $\dot{\gamma}$ = strain rate.

The first term, work hardening, is expressed as the change in shear stress with respect to strain for a given temperature and strain rate. The second term, thermal softening, is defined as the change in shear strain with respect to temperature for a given strain and strain rate. The final term, strain-rate sensitivity, is the change in stress with respect to strain rate for a given temperature and strain. The thermal softening factor in the equation is a negative value (weakening effect), which must counterbalance the positive strengthening effects, work hardening, and the strain-rate sensitivity for adiabatic shear to be induced. When the shear is induced, an instability occurs, resulting in Equation 1 being equivalent to zero. Rearranging the equation to set the thermal-softening relation (the negative value) equivalent to the work-hardening factor and the strain-rate factor (both positive), the amount of thermal softening needed to overcome the work-hardening factors for adiabatic shear to be induced is determined. Equation 2 below shows the thermal-softening relation.

$$\frac{\partial \tau}{\partial T})_{\gamma,\dot{\gamma}} dT \; = \; \frac{\partial \tau}{\partial \gamma})_{T,\dot{\gamma}} d\gamma \; + \; \frac{\partial \tau}{\partial \dot{\gamma}})_{T,\gamma} d\dot{\gamma} \; . \tag{2}$$

2

It is estimated that 90% of the work due to deformation is eventually converted to heat (Flockhart, Woodward, and O'Donnell 1990). Since these high rates of deformation occur over extremely short times, thermal conductivity is not an important parameter because there is insufficient time for the heat to be conducted away from a specific area. Heat capacity (C_p) however, is a significant parameter since it determines the amount of incremented energy required to raise the temperature in the material. Therefore, the lower the heat capacity, the more rapid the temperature rise, and the more apt a material is to exhibit a thermal softening behavior. A simplified explanation describes the onset of adiabatic shear as a plastic flow resulting when localized heating occurs faster than conductive cooling.

Adiabatic shear bands can appear in two forms. The first is a deformation band, which is the result of a very high shear in a narrow band. Inside the band the grains are highly deformed, but the structure is unchanged. In contrast, the second form, a transformation band, has a crystallographic phase change from the original material. This occurs because the heating was large enough to change the structure. These typically are evident by "white bands" after metallographic etching.

2.2 Penetration Process. As a projectile penetrates into an armor, it erodes, displacing the target material around its perimeter. The available kinetic energy (KE) of the impacting projectile is consumed either by eroding the projectile or by displacing the target material. Therefore, for an efficient penetrator, the majority of the energy should be used to displace the target material as opposed to eroding the projectile. The inverse is true if an efficient target material is desired, in which case minimal target material should be displaced, leaving penetrator erosion as the primary energy sink.

The penetrator is consumed during various phases of penetration; impact, steady-state, and final (come to rest). Long rod penetrators are primarily consumed in the steady-state phase of penetration. This phase of penetration is where the projectile erodes at a constant rate producing a constant channel diameter. The steady-state penetration is a function of rod length. As the length of the rod increases, the percentage of penetration in the steady-state phase is increased.

If the target is thin enough to be perforated by a given penetrator, the stress field in the target is converted from a primarily uniform expansion in the lateral direction to one in which free surface localizations develop as the penetrator approaches the back face of the target. The localizations manifest themselves as shear bands extending to the rear free surface, resulting in shear plugging of the rear surface. Once the shear bands have formed, the plug can be ejected with minimal amounts of energy. The influence of adiabatic shear failure in the final stage of perforating the target, referred to as plugging, has been studied by Moss (1980). Once a shear band is formed that extends to the free surface, the plugging process requires less energy than the formation of a ductile bulge. Plugging failure occurs earlier in the perforation process in proportion to the strength and hardness of the target. Hence, harder materials produce a thicker plug than softer material of similar chemistry.

2.3 Previous Research in Ballistic Shear. Adiabatic shear bands have been observed in various ballistic materials at high rates of strain. Most of the studies have concentrated on the final phase of perforating the target, otherwise known as the plugging phase. Woodward, Baxter, and Scarlett (1984) observed plugging in titanium and aluminum, where they determined the limit velocity required to perforate the target material being evaluated. A limit velocity is the velocity at which a penetrator will just perforate the target with a residual velocity of zero. The limit velocities, therefore, must incorporate the plugging or breakout of the armor as the target is perforated. Also, titanium and aluminum both have densities (4.5 g/cm^3 and 2.7 g/cm^3, respectively) much lower than steel (7.85 g/cm^3). Although these low density material diagnostics are valuable for light armor applications where the primary mode of failure is the plugging phase, they are not applicable to the heavier steel armors where deep penetration plays a significant role in the defeat of the armor.

Woodward also evaluated Hadfield steels (Yellup and Woodward 1980), demonstrating how they resist shear because of their high work-hardening rate. Hadfield steels are cold worked by rolling to achieve their higher strengths. A constant hardness through the thickness of the plate by the rolling method is only ensured for thin plates. The limited thickness forced Woodward to again determine limit velocities for the target resistance as opposed to depth of penetration measures. In addition, he used a 0.30-caliber armor piercing (AP) round, which is designed to perforate thin armors and is typically not designed for a very long steady-state penetration phase during the perforation of an armor.

4

As mentioned, Moss (1980) also observed adiabatic shear in the perforation of RHA. His work is a classic description of shear banding, but again it focuses on the final break out phase of the perforation as opposed to the actual steady-state penetration phase. The concentration on perforation as opposed to penetration is understandable in these ballistic studies because the purpose of a projectile is to completely perforate the armor. However, to reach the plugging phase in a thick armor, the penetrator first must complete the nearly steady-state penetration phase.

Adiabatic shear bands have also been observed during the steady-state penetration phase prior to plugging. However, the effects of the "internal" shear bands on target resistance to penetration have not been as thoroughly examined. For example, Meyers and Witman (1990) observed radial shear bands in low carbon content (approximately .2 weight-percent) steels, but they did not discuss the effect of the radial shear banding on the target resistance or the final depth of penetration.

This investigation compares a novel target material with two existing steel armors, rolled homogeneous armor (RHA) and high hardness armor (HHA), to examine the effect of shear banding during the steady-state penetration phase. Standard HHA is of high hardness (BHN 512) and is prone to adiabatic shear. RHA does not have as high a hardness (BHN 340) and does not form shear bands as extensively as the HHA. HHA has been observed to produce a wide penetration cavity, approximately 25% larger than that formed in RHA for similar impact conditions. However, when the target is carefully examined, it is evident that the wider penetration channel is not developed by being displaced by the penetrator, but is created by a radial shear zone which forms around the eroding penetrator. Sheared target material in the shape of small chips break loose which result in the wider penetration channel. Often these chips simply discard (fall out) from the target after the target is saw cut or sectioned, giving the appearance of a much wider penetration channel than actually displaced by the penetrator.

The effect of the penetration channel diameter on the depth of penetration is of interest to the ballistic community. The volume of an impact crater hole is proportional to the impact KE for nonshearing target materials (i.e., RHA). Therefore, a wide penetration channel will not be as deep as a narrow channel, since the energy is redistributed to creating a wider channel as

5

opposed to a deeper one. In this study, HHA plates were observed to produce wider channels; however, most of the target material along the side walls of the penetration channel was discarded due to the shear chips as opposed to lateral bulk displacement. It is unclear if more energy is consumed producing radial shear bands (i.e., HHA) or deforming the bulk deformation of the target material laterally (i.e., RHA). The energy required to form the shear bands and/or produce bulk plastic deformation in the target will be examined for the three comparable materials in this analysis. It has been proven that higher strength materials are more resistant to penetration than lower strength materials (Meyer and Behler 1990). Therefore, if bulk deformation consumes more energy than shear banding during penetration, then it follows that a high strength material which exhibits bulk deformation will have a higher resistance to penetration.

This investigation is a preliminary step in choosing a material that does not adiabatically shear at higher strengths. In addition, a material that can be heat-treated to a range of strengths is desired to separate the strength effects from the shear effects. If the material chosen does not adiabatically shear and is of similar hardness and strength to HHA, then the energy required to bulk plastically deform the target as opposed to shear can be determined. However, if the material does shear, future samples at lower strengths can be used to determine the shear effect at lower strengths.

3. EXPERIMENTAL SETUP

3.1 Target Material. Attempting to predict a material that will be resistant to adiabatic shear during the steady-state penetration phase is a complex task. All of the previous studies examined the breakout mechanisms of the target where a free surface is a contributing factor in the formation of shear bands. Therefore, the selection of a target material demonstrating shear different than RHA or HHA during penetration was based on the analysis used by Magness and Farrand (1990). These studies focused on the behavior of the penetrator where conditions were limited to a much more confined hydrodynamic component as the penetrator is forced to "back-extrude" during penetration. Magness discovered three elements to be the driving factors in the ability of the penetrator to adiabatically shear, similar to those mentioned earlier:

(1) Low work-hardening rate
(2) Low strain-rate sensitivity
(3) High thermal softening.

Although these three factors were obtained for the shear of a penetrator, they were the only reasonable constraints available in choosing the material to be evaluated for the target plate. Since the three factors listed above are required for a shearing penetrator material, whereas for this study, a nonshearing target material is desired, the properties were reversed, i.e., high work-hardening rate, and high strain-rate sensitivity, and low thermal softening. These parameters are not specific material properties, although examination of true stress-strain curves and phase diagrams does give an indication of suitable materials. A material with high thermal softening should have a stress-temperature curve with a large negative slope from the ultimate strength at room temperature to its loss of strength at a higher temperature. A phase change can also influence this loss of strength with temperature. The phase change will increase the magnitude of the negative slope, which makes the material more susceptible to adiabatic shear than if a phase change did not exist and where the strength would decrease linearly to the melting temperature. This is evident in Figure 1, which shows the loss of strength, or high negative slope, of uranium as it exhibits a phase change prior to its melting temperature. The work-hardening term can be extracted from a true stress-strain curve. As the slope of the line from the yield point to the ultimate tensile strength increases, the work-hardening rate also increases. Strain-rate sensitivity can be measured by various tensile tests at different degrees of strain, which determine the strain-rate sensitivity of the material.

In addition to the above characteristics, the armor material under investigation had to have a density comparable to standard armor steels, which have a density of 7.85 g/cm^3. As mentioned, an additional objective was to fully examine the shear mechanism and its relation to strength. Therefore, a heat-treatable alloy was also desired.

The material chosen was the nickel-based superalloy Pyromet 718. It has a similar density (8.22 g/cm^3) to armor steels and is also heat-treatable to a large range of strengths. Pyromet 718 also has a melting temperature similar to steel (1243–1344° C as compared to 1350° C for RHA). It does not have a crystallagraphic phase change, which implies a low

7

thermal softening factor (described earlier and shown in Figure 1). In addition, transformation bands will not be formed since there is not another phase available. The strain-rate effect and its work hardening was not available for comparisons due to lack of true stress-strain curves and stress-strain curves at different strain rates. The available mechanical properties for Pyromet 718, RHA, and HHA are listed in Table 1.

HHA is a high strength material with low ductility, whereas RHA has lower strength with greater ductility. The Pyromet 718 material lies between the two materials in ultimate tensile strength (UTS), hardness, and elongation, although it does exhibit a very high strength for its hardness. The tensile stress-strain curves for Pyromet, RHA, and HHA are shown in Figure 2. These curves graphically show the differences in properties listed in Table 1. Pyromet 718 is also a heat-treatable material, and, therefore, it could be evaluated at various strengths in future examinations.

A sample of the Pyromet 718 was supplied by Carpenter Technology Corporation (CARTECH) in the form of 1.5-in (38.1 mm) diameter bar stock approximately 12 in (304.8 mm) long. For consistency, two to four shots were recommended to establish a good statistical observation of the shear effect in the target. Therefore, the bar stock was sectioned into four equal lengths (3 in each) to be used as four separate targets. HHA and RHA steels were also examined in a side-by-side test of similar size material.

3.2 Penetrator Material. In order not to complicate the final target analysis, any factors that might contribute to the shear in the target by the projectile were eliminated by choosing a nonshearing penetrator material. A pure tungsten projectile was selected because it does not shear until after the rod has been completely inverted and deposited along the channel walls. Figure 3 shows the cross section of a pure tungsten material after penetration into the lower strength RHA. The extremely smooth tunnel and the incremented discard of the tungsten material behind its tail end is evidence of a nonshearing, bulk plastic deforming penetrator at the macro-scale.

Typically, the larger the penetrator and higher the impact energy, the larger the hole channel produced for a given target. To minimize any surface effects produced from the sides of the armor sample, a small scale penetrator was used, nominally 0.236 in (6 mm) diameter

8

Table 1. Tensile Material Properties for Armor Sizes Examined

	1.25-in RHA	1.25-in HHA	1.5-in Pyromet 718
Ultimate Strength (ksi/Mpa)	135/931	262/1,806	235/1,620
Yield Strength (ksi/Mpa)	119/821	212/1,462	222/1,531
Elongation (%)	18.8	10–12	9.5
Hardness (BHN)	364	512	387
Reduction in Area (%)	—	—	26
Density (g/cm^3)	7.85	7.85	8.22

by 2 in (50.8 mm) long. The length was kept at 2 in to ensure a penetration as opposed to a perforation of the target in the ordnance velocity regime.

3.3 Ballistic Setup. Testing was conducted at the Ballistic Research Laboratory (BRL) Range 110 facility. The penetrators were fired out of a 10 foot (3.28 m) long, approximately 26-mm diameter smooth-bore barrel. The penetrator was supported in the barrel during launch by a Polypropulux sabot, a four-piece plastic material with a concave front end ("windscoop") which causes it to separate after exiting the gun and not interfere with the penetrator/target interaction. A Polypropulux obturator, following the sabot, seals the gases behind the launch package to accelerate the projectile to the required velocity. A steel pusher plate embedded in the obturator distributes the launch forces over a wider area, preventing the penetrator from setting back into the obturator and degrading the launch conditions of the rod. A sample launch package is shown in Figure 4.

The velocity of the projectile at the time it impacted the target was determined via a flash radiographic (x-ray) procedure, standard for terminal ballistic test (Grabarek and Herr 1966). Two orthogonal images of the projectile just prior to impact show the position of the projectile at preset times. The true location of the projectile was determined with fiducial wires, permitting the velocity and orientation of the projectile to be calculated. Figure 5 shows a schematic of the flash x-ray recording system for this series of experiments. A sample radiograph of a projectile prior to impacting the target is shown in Figure 6.

The penetration phase into a semi-infinite armor must not be affected by the free surfaces of the target (i.e., bulging or cracking of the rear or side free surfaces). A stress release could occur if the sides or rear are cracked or bulged, producing an unrealistic measure of the penetration. Also, if the channel is too near to a side, it will depart from its original path and veer towards the free surface. To guarantee no free surface effects, an infinitely large target material in all directions is required. Obviously this is not possible; therefore, an approximation or semi-infinite armor is used. Typical armors are cut to sizes of exaggerated proportions. For example, a 6-in cube is used for model-scale (65 g, 3.75-in-long by 0.25-in diameter rod) experiments. The small diameter of the Pyromet 718 bar stock supplied required that either the size of the projectile must be extremely small (probably less than 0.1 in) making the shear analysis more difficult, or an additional means of a confinement for the bar stock. In this study, a confinement fixture was used to ensure the largest possible volume for subsequent metallurgical examination. Holes of slightly smaller diameter than the bar stock (<1.5 in) were drilled in a 3-in-thick RHA plate (similar to the thickness of the bar stock). The plate was heated to enlarge the holes, and the Pyromet 718 bar stock cylinders were placed inside while the plates cooled to their original size. The heat-shrinking technique fully confined the material around the diameter and reduced the free surface effects, minimizing any cracking. The prestress of the Pyromet bar stock was assumed negligible for these tests. Figure 7 shows a photograph of a cylinder in the full confinement of the RHA target prior to testing.

The RHA and HHA material were examined in a similar orientation and confinement as the Pyromet 718 bar stock to constitute an equivalent comparison. RHA and HHA are available in plate and not in bar form. The closest matching available sizes of RHA and HHA to the 1.5-in-diameter Pyromet 718 bar stock were plates 1.25 in thick. HHA targets range in thickness from 0.25 in to 2 in, with a consistent hardness (BHN 477-512). However, the RHA increases in hardness as thickness decreases, with 1.25-in-thick plates having a hardness of BHN 340. These target plates were shot on the edge parallel to the rolling direction, as shown in the schematic in Figure 8, which simulates the orientation of the Pyromet 718 bar stock. Adjacent plates were clamped on both sides of the finite plate to ensure confinement in the lateral direction (shown in Figure 8).

10

4. DATA REDUCTION TECHNIQUE

Once the tests were conducted, the targets were removed from their confinements (HHA and RHA) and/or cut out of the larger piece of armor material (Pyromet 718). To examine the penetration holes, the blocks were cut along the shotline of the penetration channel, using an electric discharge machine (EDM) (through The Johns Hopkins University contracted to Suburban Tool Manufacturing Company). It was desirable to use the EDM rather than a conventional cutoff saw because the EDM process generates little heat and cold working to the sample during sectioning. However, without the knowledge of the author, the contracting facility added lead to the holes to ease the EDM machining. The low melting temperature of the lead alloy probably did not influence the microstructure of the armor materials being examined.

The cross sections of the tunnel channel were measured for typical ballistic measures and were also physically examined for any "macro" analysis of shearing. The standard ballistic measure of a semi-infinite target performance is the depth of penetration in the armor. The depth of penetration is inversely related to the target material's resistance. As the hardness is increased, the depth of penetration is typically decreased; it is much more difficult for the penetrator to "burrow" into a harder, higher strength target than a softer lower strength material at ordnance velocities (Meyer et al. 1990). A secondary measure of ballistic performance is the diameter of the channel. The diameter is directly used to calculate the volume displaced in the target by assuming a cylindrical shape and calculating volumes for finite increments of the channel. As mentioned earlier, the volume displaced should be a constant for a given amount of energy; hence, a deeper channel will have a smaller diameter. This assumption, however, does not account for the shear in the target. Therefore, for the target materials that do shear, measurements were taken both at the outermost edge of the channel diameter and the estimated inner diameter of the displaced material (penetrator/target interface).

Often the size of the shear chips are "macro" in size and can be clearly identified without extensive metallurgical examination. However, to gain a further understanding of the shear in the target (i.e., size of chips, orientation of bands, and the lateral displacement of these bands), a cross section of each specimen was polished and etched. After metallurgical

11

preparation, the section was examined with an optical microscope in search of evidence of adiabatic shear bands. Submersing the specimen for 15 s in a Nital etch was used to produce the micrographs of the RHA and HHA targets. However, the Pyromet 718 alloy is a high temperature noncorrosive superalloy and is difficult to etch. The final micrographs of this material were produced by swabbing glyceria etchant (15 parts glycerine, 10 parts HCl, and 5 parts HNO_3) onto the surface, recommended by Bob Novak, a metallurgist from the CARPENTER Technology Corp.

5. RESULTS

An important factor in properly determining the ballistic resistance of the target is the orientation of the impacting projectile. Penetrator yaw is defined as the angle between the longitudinal axis of the penetrator and the velocity vector. The higher the L/D ratio, the more sensitive the projectile's penetration performance is to unfavorable impact orientation (Bjerke et al. 1991). A yaw less than 2.0° is acceptable for the L/D of 8.5 used in this study, although the lower values may improve the penetration slightly. The yaw values were recorded and noted for each of the tests performed.

Table 2 lists the impacting conditions (velocity, yaw, length, mass, and KE of the rod) along with the post-mortem target measures. The postmortem measures include the depth of penetration (DOP), channel diameters (Dt-unsheared portion and Dts-sheared section), hole volumes (Vt- unsheared and Vts- sheared portion), and KE per channel volume (KE/Vol). From the table, it is evident that the impact yaws were acceptable for all of the tests. However, shot numbers 4044 into HHA and 4047 for the Pyromet 718 are at the upper limit of yaw and should be treated with caution. It was desired to impact the targets at two velocities, 1,250 m/s and 1,400 m/s. To ensure repeatability, an additional penetrator was shot at 1,400 m/s into the Pyromet 718 target. Obviously, there are small deviations from these velocities in the actual tests; however, they are within an acceptable range. By using two velocities with a 200 m/s separation, a curve of velocity vs. a parameter of interest could be constructed. Assuming the data follow a fairly consistent trend, the individual curves for each material can then be compared at any specific velocity within the velocity range.

12

Sample pictures of the Pyromet 718 confined targets after testing are shown in Figure 9. Even with the highly restrained confinement configuration used, there were obvious signs of cracking that extended to the outer edge of some samples. However, for the one shot where the impact was dead center (number 4047), there does not appear to be any cracking. The photograph of the RHA and HHA plates, shown in Figure 10, also show some minor cracking and bulging along the edges. The influence of the exterior cracks (perhaps a stress release) on the depth of penetration cannot be assessed at this point. Detailed micrographs of sectioned targets, along with an analysis of each, will be addressed in the following section.

6. DISCUSSION

If the adiabatically sheared "chips" in the target material do indeed exist, they can be observed from the target half-section on the "macroscale." Photographs of the RHA half-sectioned blocks are shown in Figure 11. The characteristic nonshearing behavior of the pure tungsten penetrator is evident. The penetrator exhibits a large degree of bulk deformation as it back extrudes around the incoming rod. Only after it is completely inverted does it show signs of shearing, as illustrated by the incremented "waves" of inverted tungsten material. The remaining aft end of the penetrator is still completely intact and undeformed. The smooth tunnel walls of the RHA target also confirm the nonshearing nature of the target. However, there is some evidence of minimal cracking and/or formation of shear bands along the edge of the walls.

The photographs of the HHA half-sections are shown in Figure 12. The large sheared chips lining the channel walls of the HHA plate are true indications of a shearing material, especially notable in shot number 4044, impacted at 1,391 m/s. For this shot, there is a distinct difference between the penetrator and the shear-affected zone in the target. In contrast, the sheared HHA chips for shot number 4043 (impacted at 1,228 m/s with considerable yaw) are intermingled with the back extruded tungsten penetrator, and hence, there is not a recognizable boundary between the penetrator and target material. Shot 4043 also exhibited severe cracking extending to the outer edge of the target, perhaps influencing the back flow of the penetrator material. It is difficult to determine whether the sheared chips interfered with the back-extruding material for these two shots. However, the affected shear zone for the HHA is considerably larger for both shots than for the RHA targets.

13

Table 2. Ballistic Shot Data

Shot No.	Material	BHN	Mass (g)	Length (mm)	Velocity (m/s)	KE (kJ)	Yaw (deg)	Pene (mm)	Dt (mm)	Dts (mm)	Volt (cm³)	Volts (cm³)	KE/Vt (kJ/cm³)	KE/Vts (kJ/cm³)
4041	RHA	340	29.1	2.10	1,241	22.4	1.41	39.1	11.2	—	3.9	—	5.8	—
4042	RHA	340	29.1	2.11	1,417	29.2	0.25	52.3	11.7	—	5.6	—	5.2	—
4043	HHA	477	29.9	2.10	1,228	22.5	0.90	30.0	NM	15.5	—	5.7	—	4.0
4044	HHA	477	29.0	2.10	1,391	28.1	2.00	41.2	9.7	16.5	3.0	8.8	9.2	3.2
4045	Pyromet 718	387	28.9	2.10	1,266	23.2	0.25	36.6	8.4	13.2	2.0	5.0	11.4	4.6
4046	Pyromet 718	387	29.2	2.10	1,432	29.9	0.75	47.8	10.2	12.7	3.9	6.1	7.7	4.9
4047	Pyromet 718	387	29.0	2.10	1,381	27.7	1.75	43.2	8.9	13.2	2.7	5.9	10.3	4.7

The photographs in Figure 13 show the three Pyromet 718 target sections. Some variability in the target behavior is evident from these photographs. Shot numbers 4045 and 4047 impacted at 1,266 m/s and 1,381 m/s, respectively, show the tungsten material surrounded by a sheared portion of target material, similar to HHA but not to the same extent. Shot number 4046, at the highest velocity (1,432 m/s), is vastly different from the other two Pyromet 718 shots. Although shear bands have formed in the target channel, they do not connect to form the larger chips indicative of the other two shots, which implies a much smaller affected area.

6.1 Microanalysis. As a result of the highly dynamic nature of the penetrator/target interaction, small amounts of material remain loose along the penetration channel. After the blocks are cut along the shotline, EPOXY was added to prevent the loose material from being worked free during the finer stages of the polishing. The EPOXY is still visible in each of the half-sections after the final polishing phase was completed. An enlarged view of each half-section was produced to serve as a guide for locating the position of each micrograph and its orientation (matching direction of the arrows) taken thereafter. All micrographs are taken with a magnification of 250x.

6.1.1 RHA Microanalysis. The first section examined was shot 4041, RHA impacted at a velocity of 1,241 m/s, shown in Figure 14. This enlarged view shows the penetrator lodged in the bottom of the channel with the tail end still intact. Also, the smooth surface of the target channel walls are evidence of a nonshearing target and penetrator material. For a comparison point, a micrograph of the virgin RHA material was taken a sufficient distance away from the penetration channel (location 1 marked on the macro photo and shown in Figure 15). The micrograph shows the original microstructure of the RHA and its random orientation of the grains. A second micrograph, along the edge of the tunnel (location 2 marked on the macro photo and shown in Figure 16), shows the highly deformed material as it is developing into a localized deformation band. The original microstructure is no longer detectable, and the grains are highly elongated and oriented in a particular direction. Figure 17 shows the microstructure inside the one visible chip (location 3 on the macro photo). Again, the grains are highly deformed, and it is likely that the deformation occurred prior to being chipped away from the remaining RHA.

15

The second RHA half-section, shot number 4042 impacted at 1,417 m/s, is shown in Figure 18. As in shot 4041, the tail end of the penetrator is still intact at the bottom of the channel, and the channel walls appear smooth. Some shear cracks along the walls are more evident in this shot than 4041, perhaps due to the higher impact velocity. The highly deformed grain structure adjacent to the channel wall is evident in Figure 19 (location 1 on the macro photo). Figure 20 shows the end of a deformation band being formed along the edge of the channel (location 2 on the macro photo). The material is extremely deformed as the band is developed here also. Another micrograph of a shear band is shown in Figure 21 (location 3 on the macro photo). Here again the material to either side of the band is highly deformed prior to the localization being developed. A micrograph taken directly in front of the head of the penetrator is shown in Figure 22 (location 4 on the macro photo). The microstructure is highly oriented and compressed. Figure 23 (location 5 on the macro photo) shows that as the distance from the head is increased, the degree of compression and orientation is decreased. Overall, the micrographs demonstrate that an extremely high degree of bulk plastic deformation has occurred in the RHA samples and that a minimal amount of shear banding is evident.

6.1.2 HHA Microanalysis. The first HHA half-section examined, shot number 4043 impacted at 1,228 m/s, is shown in Figure 24. The enlarged view shows considerable amounts of tungsten penetrator and HHA chips intermingled as the penetrator back extruded. This effect could be attributed to the large crack extending to the edge of the plate, introducing a free surface and perhaps a stress relief. This cannot be quantified, however, by only one shot. An undeformed region, location 1, is shown in Figure 25. The randomly oriented high hardness martensite is evident in the micrograph. Figure 26 is a micrograph of the area directly in front of the penetrator head (location 2 on the macro photo). Here, in contrast to the highly deformed material observed in the RHA, a white shear band (transformation band) appears in the midst of virtually undeformed HHA material. Such a microstructure implies that the strain is concentrated in the localized shear band and does not produce the extreme amount of bulk plastic deformation seen in RHA. Two views inside the actual chips are shown in Figures 27 and 28 for locations 3 and 4 on the macro photo, respectively. For both of these micrographs, many transformation bands surrounded by virtually undeformed material, similar to Figure 26, are seen. The large number of bands surrounded by undeformed material is another indication of highly strained material where the

16

strain is localized in the bands and the remaining material is not affected. The numerous bands located in a similar size area as seen in Figure 26 imply that the chips were subjected to higher degrees of strain than the area in front of the penetrator head.

The last HHA shot evaluated was number 4044, impacted at 1,391 m/s, and is shown in Figure 29. As in the RHA, the rear of the penetrator is undeformed. The enlarged view also shows a distinct boundary between the inverted penetrator material and the HHA chips aligning the walls. Many of the chips run parallel to the walls with one or two chips turned perpendicular. There does not appear to be any chips produced directly in front of the penetrator, although some shear bands are evident. Micrographs of the shear bands around the periphery of the tunnel are shown in Figures 30 and 31, locations 1 and 2 on the macro photo, respectively. Similar to shot number 4043, the strain seems to be concentrated in the band with the adjacent area virtually undeformed. A micrograph of a chip, Figure 32 at location 3 on the macro photo, shows the undeformed material without bands. The larger size of the chip may explain the absence of bands as observed in the smaller chips shown earlier.

6.1.3 Pyromet 718 Microanalysis. The Pyromet 718 material deformed in a manner different from either the HHA or RHA. Figure 33 shows an enlarged view of shot number 4045, which had an impact velocity of 1,266 m/s. There are indeed shear chips but not to the extent as in the HHA material. Figure 34 is a micrograph of the undeformed area (at least undeformed by the penetrator) for the Pyromet 718 bar stock (location 1 on the macro photo). The highly oriented microstructure due to the rolling of the bar prior to testing is evident by the elongated grains being parallel to the length of the bar stock (rolling direction). The structure also does not have the martensite as seen in the HHA, because it is precipitation hardened and rolled to achieve desired strength. Figure 35 shows an interesting view located directly in front of the penetration channel (location 2 on the macro photo). The grains change orientation, indicative of the bulk plastic deformation observed with the RHA but not as prominent. The grains are again highly oriented along the edge of a material chip and adjacent to the tungsten material as seen in Figure 36 (location 3 on the macro photo). In addition, the material in the upper right-hand corner appears to be recrystallized. This is certainly expected since Pyromet 718 is known to recrystallize at extremely high rates of strain (Donachie 1984).

17

The other Pyromet 718 shot with similar features, shot number 4047, impacted at 1,381 m/s, is shown in Figure 37. The variations in deformation are demonstrated in this section in Figures 38, 39, and 40, located at increased distances from the head of the crater (locations 1, 2, and 3 on the macro photo), respectively. The grains change orientation as their distance from the channel is increased. The material is highly strained at the penetrator/target interface (Figure 38) and decreases in strain as the microstructure returns to the original form further away (Figure 40). Another view of the interaction of various formed chips is shown in Figure 41 (location 4 on the macro photo). Again the microstructure is severely deformed, especially at the edge of the chips. Location 5 on the macro photo, Figure 42, shows the inside of a chip located along the edge of the penetrator/target interface. Here also, the grains are deformed and directionally oriented.

The final Pyromet 718 target, impacted at 1,432 m/s, is shown in Figure 43. The enlarged view shows that many bands are visible along the edge of the channel, but they are not continuous as was seen in the previous targets. Figure 44 (location 1 on the macro photo) is a view of several deformation bands along the edge of the tunnel. The extreme orientation of the grains which accompany the actual band forming is confirmation that these are not as highly localized as observed in the HHA, but are formed after large bulk deformation, similar to RHA. Location 2 in Figure 43 (Figure 45) shows another view of the edge of chips. It appears that the chips slid past one another since the orientation of the grain structure on each side of the band is dissimilar.

6.1.4 Microanalysis Comparison. For all three materials, filling the penetration tunnel with lead did not appear to have any influence on the microstructure. Again, this is probably due to the much lower melting temperature of the lead alloy.

The deformation of the three materials examined by the micrographs is drastically different. The RHA material is highly deformed as the microstructure goes from randomly oriented grains to a compressed and directionally oriented microstructure near the strained regions adjacent to the penetrator/target interface. The HHA, in contrast, is typically undeformed with no large amounts of bulk plastic deformation. The strain in the HHA is concentrated in a localized shear band, which forms chips along the channel walls. The Pyromet 718 material responds in a manner between HHA and RHA. It shows bulk plastic

18

deformation along the interface with the penetrator, similar to the RHA, and it also forms a more localized band, similar to the shear bands observed for the HHA. The bands in the Pyromet 718, however, are deformation bands, resulting from the deformation of the surrounding material and are not as localized as the transformation bands observed in the HHA.

6.2 Ballistic Analysis. As mentioned, the ballistic data can be graphically depicted as a function of velocity for the purpose of data comparisons. Figure 46, a plot of impact velocity vs. final depth of penetration, shows the relative ballistic performance of each target material. As the impact velocity increases, the depth of penetration also increases for the three different materials. Since higher target resistance will yield lower depth of penetration values, the HHA is the most resistant, RHA is the least resistant, and the Pyromet 718 resistance lies in the middle. The increased resistance of the HHA is expected because of its higher hardness and strength. To further illustrate the hardness effect, a plot of depth of penetration as a function of target hardness is shown in Figure 47. Two curves are constructed with three points each. The lower curve is for an average velocity of 1,245 m/s, and the upper curve is for an average of 1,405 m/s. The curves are not linear, but the trend in depth of penetration with hardness is evident. A similar plot of depth of penetration as a function of ultimate tensile strength is shown in Figure 48. Again, the same trend is evident. Although these plots illustrate the effect of target strength on penetration, the effect of shear bands on penetration performance is not readily deduced.

As seen from the earlier photographs, the diameter of the affected area and the back-extruded penetrator may give some insight to the material's shear tendencies and the way it influences the target resistance. This data is best illustrated in the form of a plot of channel diameter as a function of impact velocity, shown in Figure 49. Two symbols for each target are shown; the solid symbol is the measured diameter of the back-extruded penetrator, or unsheared area, and the open symbol is the measured diameter of the shear-affected area. Although the area around the periphery of the channel is obviously affected by severe plastic deformation for the RHA, the actual diameter of this area cannot be determined. Therefore, the two points for the RHA coincide. In contrast, for the one HHA shot where a distinct penetrator diameter was identifiable (shot number 4044), the gap is considerably larger. The penetrator-displaced region for the other HHA shot was not distinguishable from the shear-

19

affected area. The Pyromet 718 has a slightly smaller gap between the penetrator and sheared zone. The one outlier is the Pyromet 718 target impacted at 1,432 m/s (shot number 4046). There is only a slight increase in diameter for the sheared zone, in agreement with the micrographs. It appears that the shear zone is decreasing with velocity, although there is insufficient data to draw firm conclusions.

The data used in the diameter and depth plots, Figures 49 and 46, are combined to calculate the volume of the semi-infinite craters. Incremental diameter measurements were made along the penetration channel, and by assuming a cylindrical channel, the volumes were calculated by summing the area times depth (volume) of the individual increments. Figure 50 shows the measured volumes plotted as a function of impact velocity. If the shear effects were negligible, the harder steels would lie lower on the curve where more energy was consumed, plastically deforming the higher strength material. This is possibly indicative of the unsheared data (solid points) on the plot, where the HHA and Pyromet 718 lie lower than the RHA. However, the separation of the curves implies some shear effect. The three points for the unsheared portion of the HHA and Pyromet 718 lie along a horizontal line. For the few points available, a constant volume with respect to velocity cannot be deduced. Normalizing the target volume by the KE impacting the target, the values should be constant (perhaps slightly decreasing). This is indeed the case for the RHA and HHA, with the HHA being slightly lower due to its higher strength (See Figure 51). The higher the data lies on the plot, the more energy is consumed to create a given amount of volume in the target. The HHA is lowest on the curve which implies that it consumes more energy to produce the same volume hole as compared to the other armors. The Pyromet 718 data are very inconsistent. As the velocity is increased, the KE/volume increases slightly, giving the impression of a less efficient target at higher velocities for the sheared areas. Again, the limited data does not warrant a definitive conclusion.

The ballistic results show how the data can be construed. If the shear affected area in the target (outer edge of the shear chips, i.e., HHA) or just the displaced target material is used to determine the efficiency (KE consumed) of the target, the conclusions may be reversed. When the sheared volume is used, the HHA appears to be less effective; however, its penetration is still lowest. If the displaced material is compared, the RHA is less effective. Therefore, if the KE/volume measure is to be used as the comparison factor, the area to be

20

measured must be determined prior to testing. Again, the primary measure in penetration is the depth of penetration. This should be the deciding factor for an armor's effectiveness.

7. CONCLUSIONS

The dynamic deformation behaviors resulting from penetrating impacts was examined for three different target material samples. The RHA exhibits bulk plastic deformation, where the grain structure becomes highly strained and directionally oriented around the periphery of the hole. Conversely, the HHA exhibits an undeformed microstructure with the high strain being concentrated in localized adiabatic shear bands. The Pyromet 718 superalloy shared deformation qualities of both RHA and HHA. The original, highly orientated microstructure of the Pyromet 718 becomes deformed and reoriented, but not to the extent of RHA. The Pyromet 718 deformation was more concentrated than in the RHA and most likely an indication of localized deformation bands.

The effect of the deformation mechanism on the ballistic penetration resistance of HHA, RHA and Pyromet 718 is not easily assessed. Not only were the modes of failure different for the three materials, but the material properties also varied. This did not permit a side-by-side comparison as originally planned. However, some terminal ballistic effects are still evident. Obviously the softer, lower strength RHA is less resistant to penetration and the harder, higher strength HHA is most resistant to penetration. The Pyromet 718 alloy, of moderate hardness with fairly high strength, lies between the resistance performance of the two other armors. Since the Pyromet 718 alloy is not an iron-carbon steel and its hardness-to-strength ratio is different from that of steel, its penetration resistance does not follow the same form for both hardness and ultimate strength with RHA and HHA. Another factor not considered is the reliability of the material properties used in the analysis. Although the hardness tests were performed on the sample just prior to testing and are actual values, the other material properties were material specifications and were not actually measured for each sample tested.

The volume displaced to produce the penetration channel for a given impact KE is dependent on which volume was measured. The volume could be measured by the displaced target material (volume occupied by the tungsten penetrator) or measured by the total sheared

21

or affected zone around the penetration channel. The shear affected zone in the RHA was minimal and, therefore, could not be measured separately. However, it was determined for the more distinct shear chips in the HHA and Pyromet 718 materials. When the volume was measured based on the inner diameter of the unsheared zone, it appeared that the penetrator requires more energy to produce the crater volume in HHA. However, if the energy was normalized by the affected sheared volume, then the penetrator required more energy to produce a crater in the RHA target. These differences in distribution of energy must be analyzed as new target materials are being explored. The decisive factor in armor performance is its resistance to penetration and it appears that the higher the ultimate strength, the more resistant it is to penetration.

8. RECOMMENDATIONS

This study has addressed the various failure mechanisms in HHA, RHA, and Pyromet 718 impacted with KE penetrators producing strains on the order of 10^5. The different mechanisms could not be directly related to ballistic penetration resistance because of the range and variation in material properties. Future studies will be conducted which examine a material of either lower strength, similar to RHA, or high strength, similar to HHA, that exhibit failure modes different than those already observed. Other possibilities are to establish curves for RHA or HHA of higher or lower strengths, respectively. This would allow the determination of the relative performance of newer alloys (i.e., Pyromet 718).

It is also recommended that a material be tested that is easily strengthened (perhaps mild steel). It could be evaluated using ballistic impact experiments at different strengths (heat treatments) to determine if the material goes from a bulk plastic deformation to a localized shear deformation. This would be evident by a jump or discontinuity in depth-of-penetration plots. If there is indeed a discontinuity, then the shear failure mechanism as opposed to the bulk plastic deformation can be modeled.

Material properties have been listed that would produce adiabatic shear in a material or produce bulk plastic deformation. Most of these properties are not readily available and are difficult to measure; therefore, until cheaper methods of determining thermal-softening, work-hardening, and strain-rate sensitivity are developed, the trial and error method of determining

the ability of a material to adiabatically shear is unavoidable. If materials comparable in strength and density can be found that shear or resist shear, then the determination of the energy consumed in displacing the material with respect to localizing the strain can be better resolved and quantified.
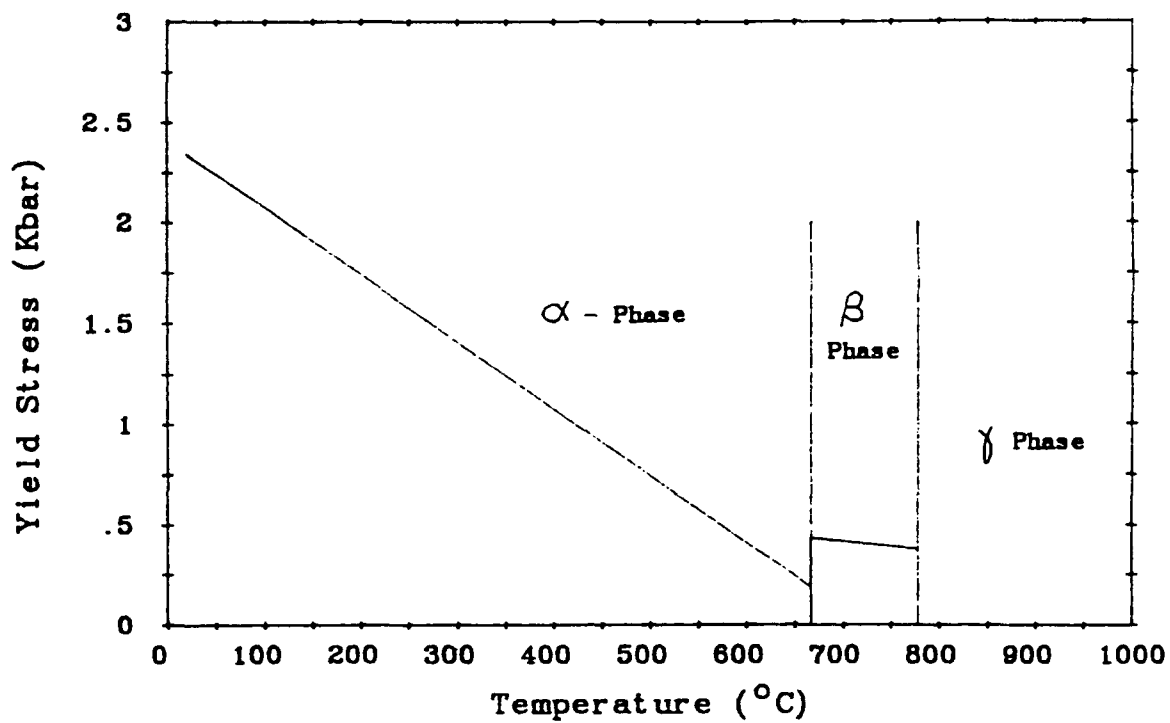
Figure 1. Strength as a Function of Temperature for Uranium.
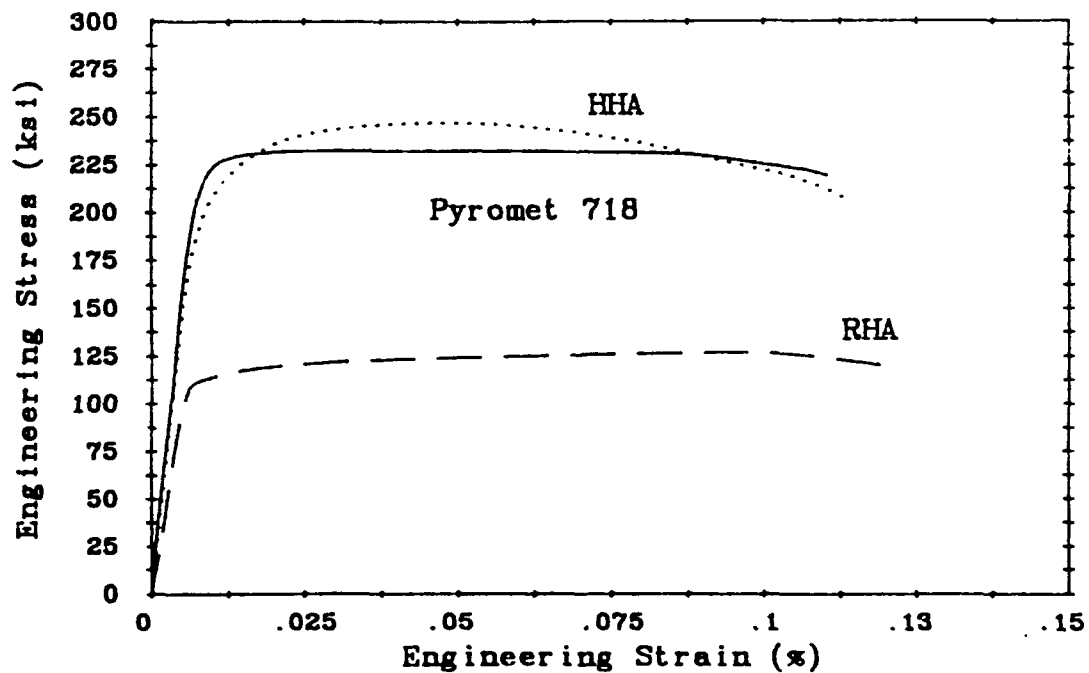
Figure 2. Engineering Stress-Strain Curves for RHA, HHA, and Pyromet 718.

24

Figure 3. Cross Section of a Pure Tungsten Penetrator.

Obturator   Pusher   Sabot
             Plate
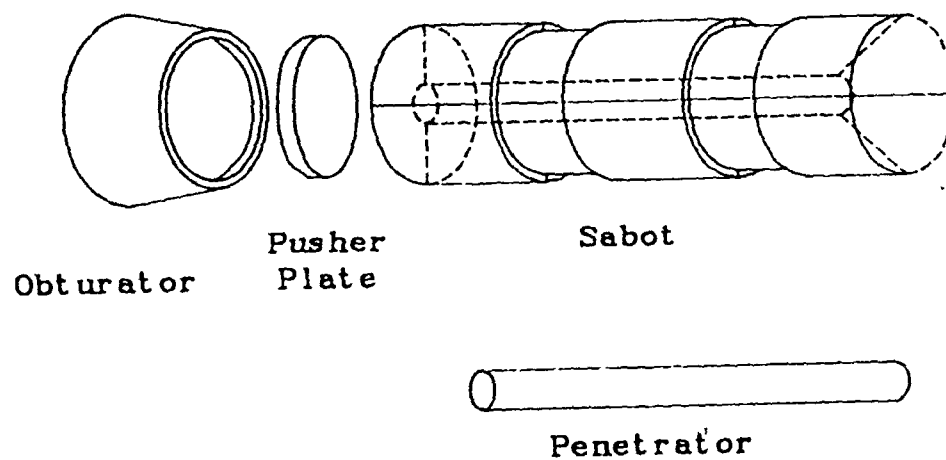
Penetrator

Figure 4. Ballistic Launch Package.

25
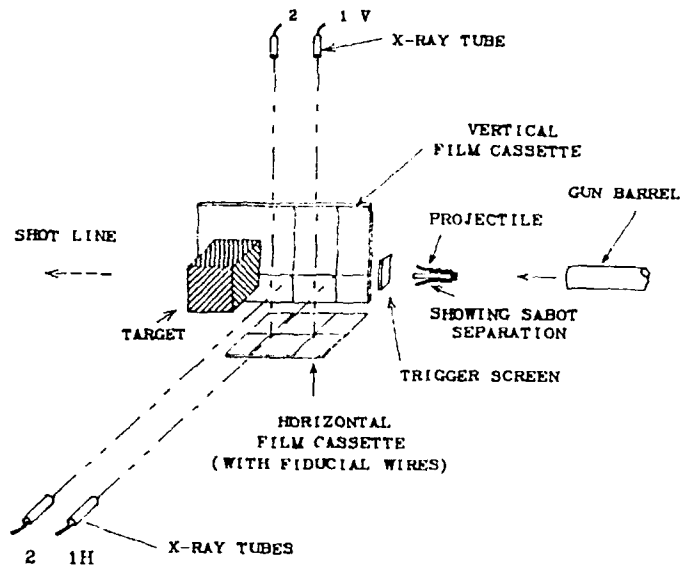
Figure 5. Schematic of Radiographic Setup.

Note: Projectile is Traveling Right to Left.

Figure 6. Sample Radiograph of Pre-Impact Penetrator.

26
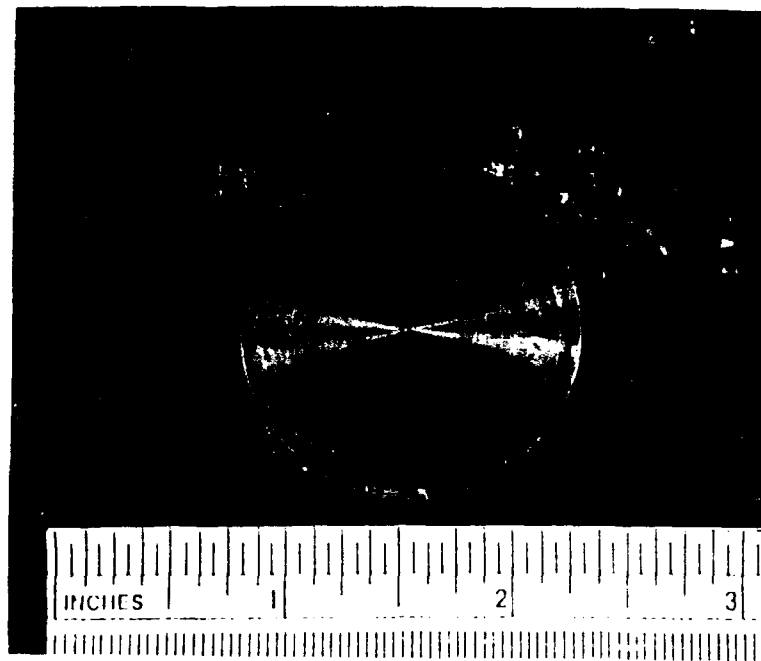
Figure 7. Photograph of Pyromet 718 Bar Stock Confined in RHA Plate.

3 - 1.25-in-thick target plates
Clamped together for confinement

6"

18"

Shot Location
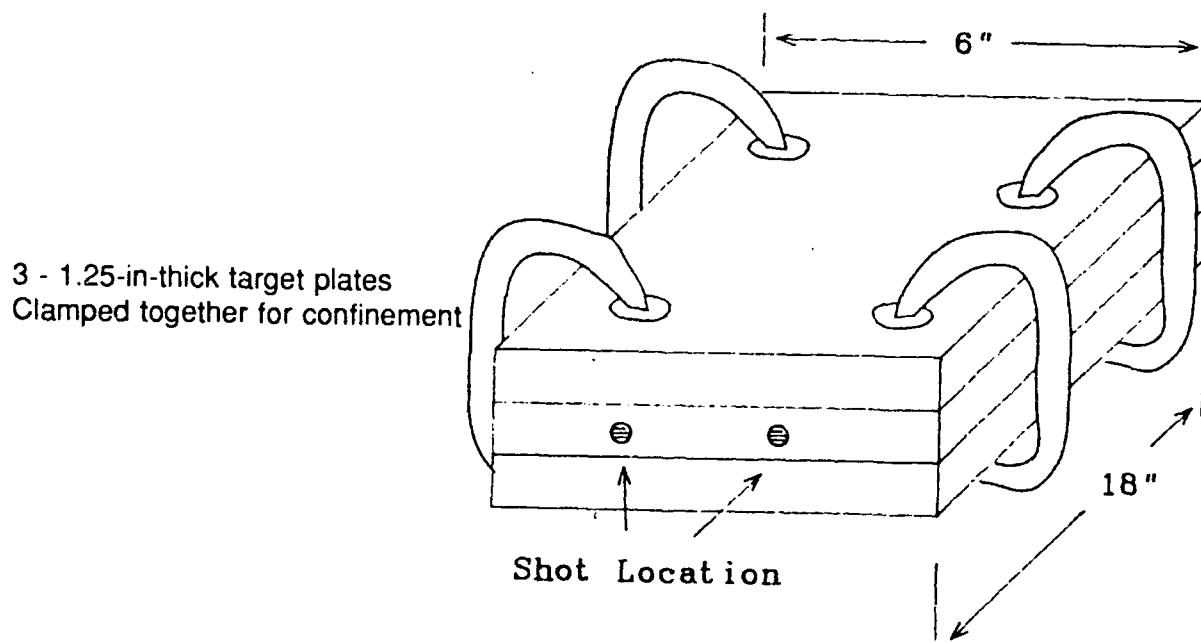
Figure 8. Schematic of Confinement Used for RHA and HHA Targets.

#4045

#4046

#4047

Figure 9. Photograph of Impact on Pyromet 718 Targets.
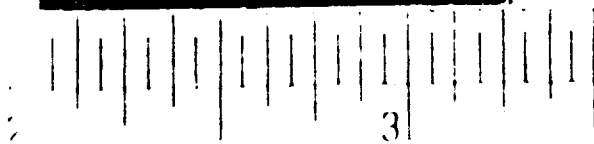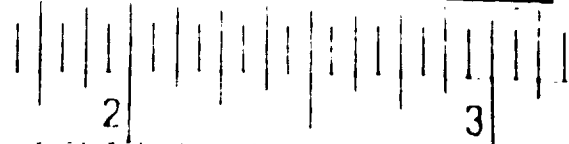
#4041   #4042

(RHA Targets)
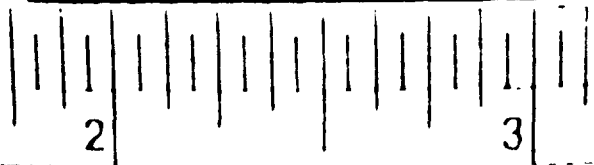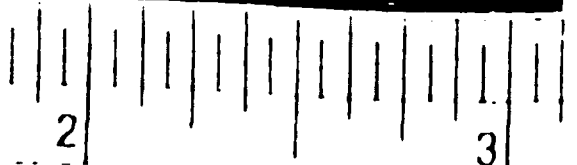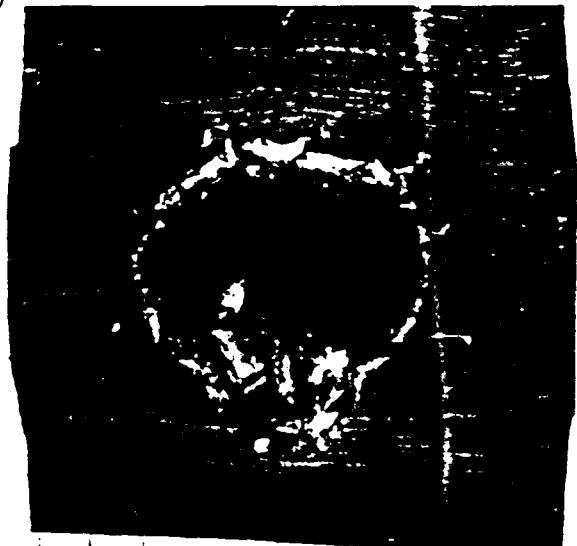
#4043   #4044

(HHA Targets)

Figure 10. Photograph of Impact on RHA and HHA Target Plates (Continued).

29
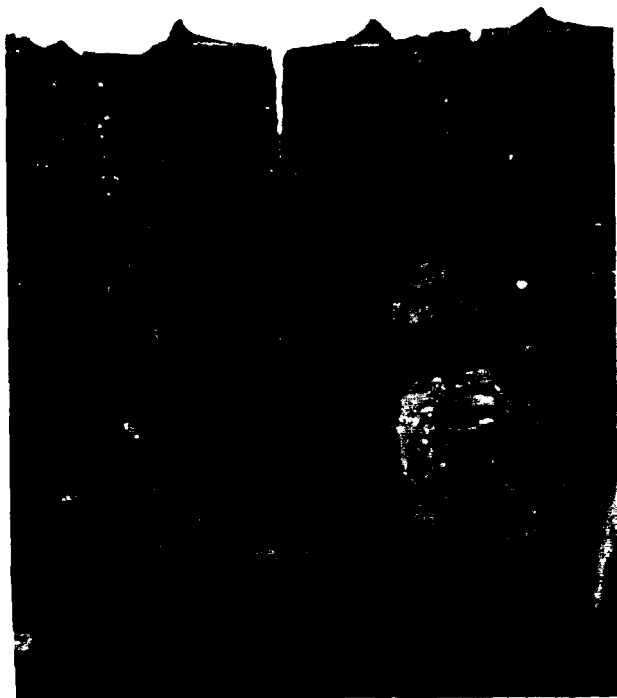
#4041
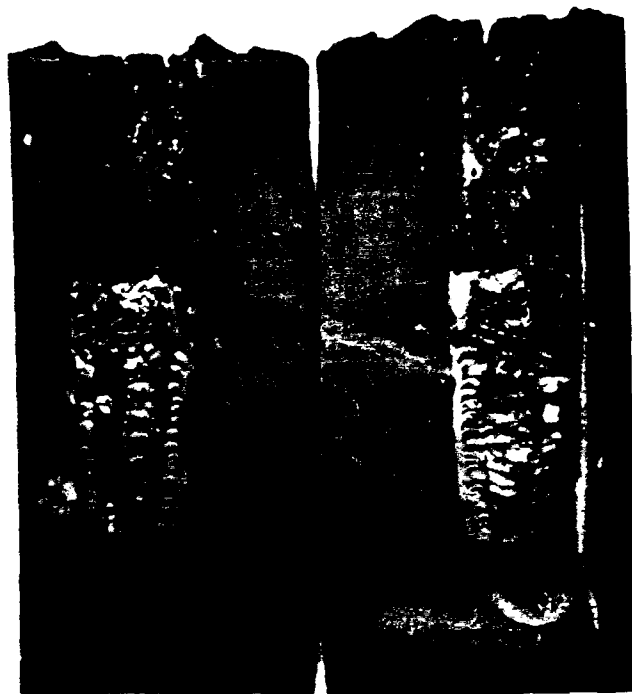
#4042

Figure 11. Photograph of Half-Section of RHA Plates.

#4043
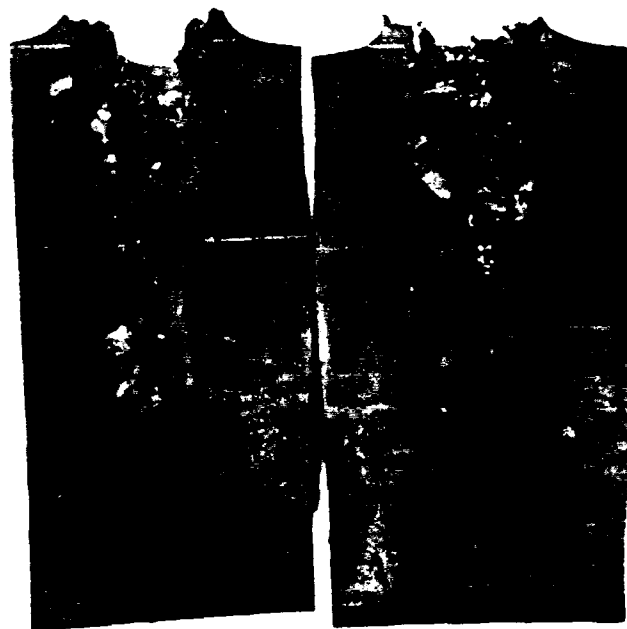
#4044

Figure 12. Photograph of Half-Section of HHA Plates.

30

#4045
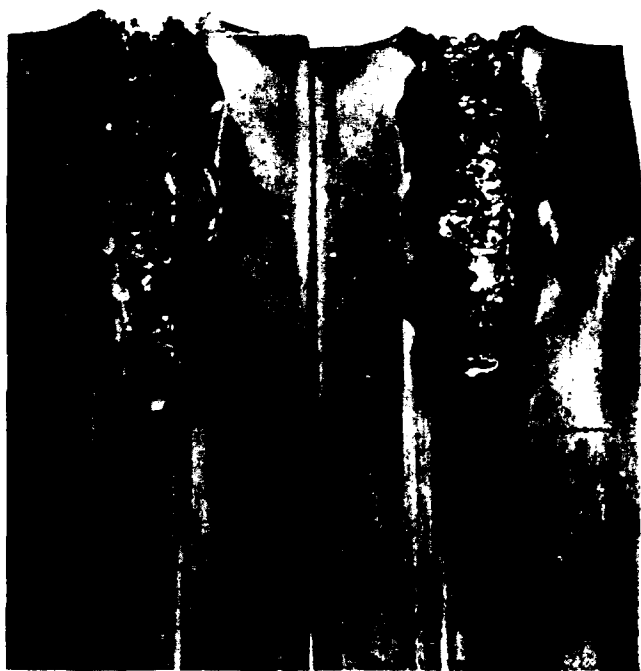
#4046

#4047

Figure 13. Photograph of Half-Section of Pyromet 718 Plates.

Arrow indicates
flight direction

2

3

1

INCHES
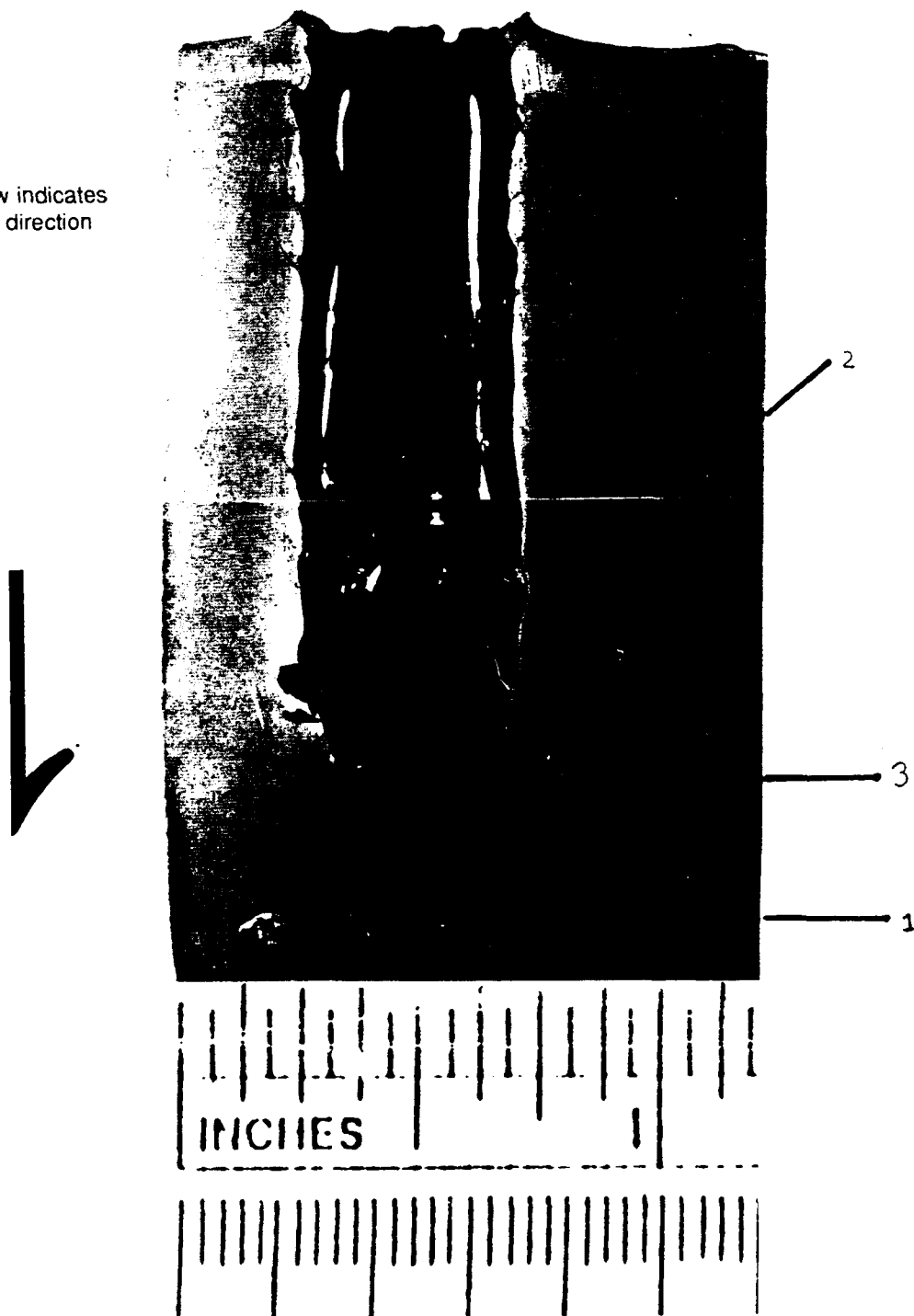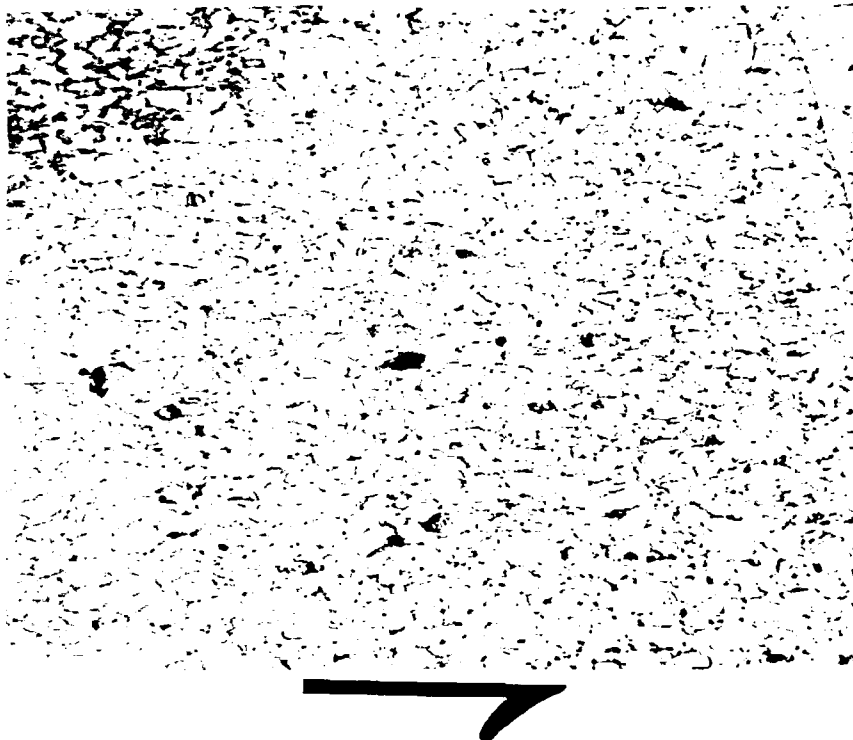
Figure 14. Enlarged View of RHA Target, Shot Number 4041.
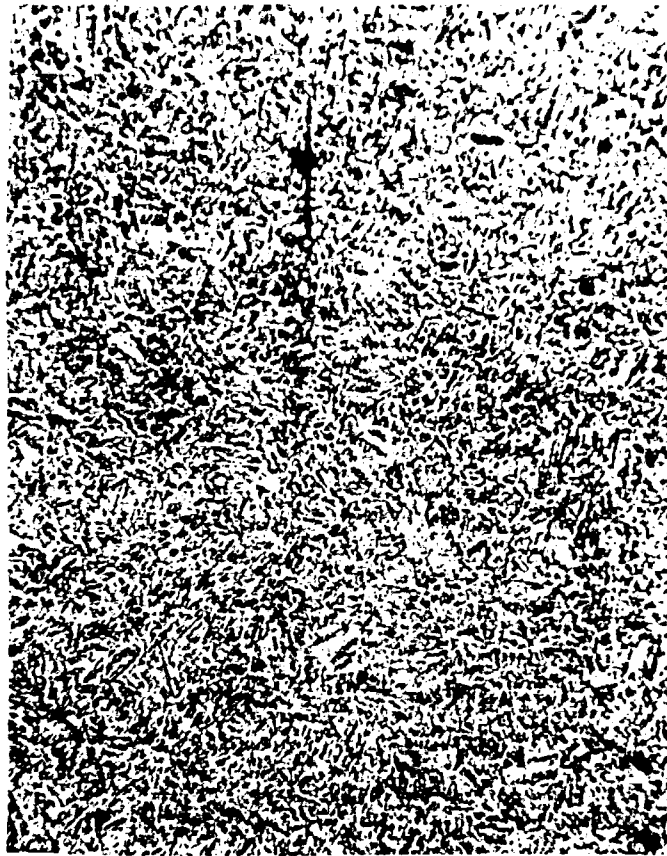
Figure 15. Micrograph of Virgin RHA Material (No. 1 in Figure 14).

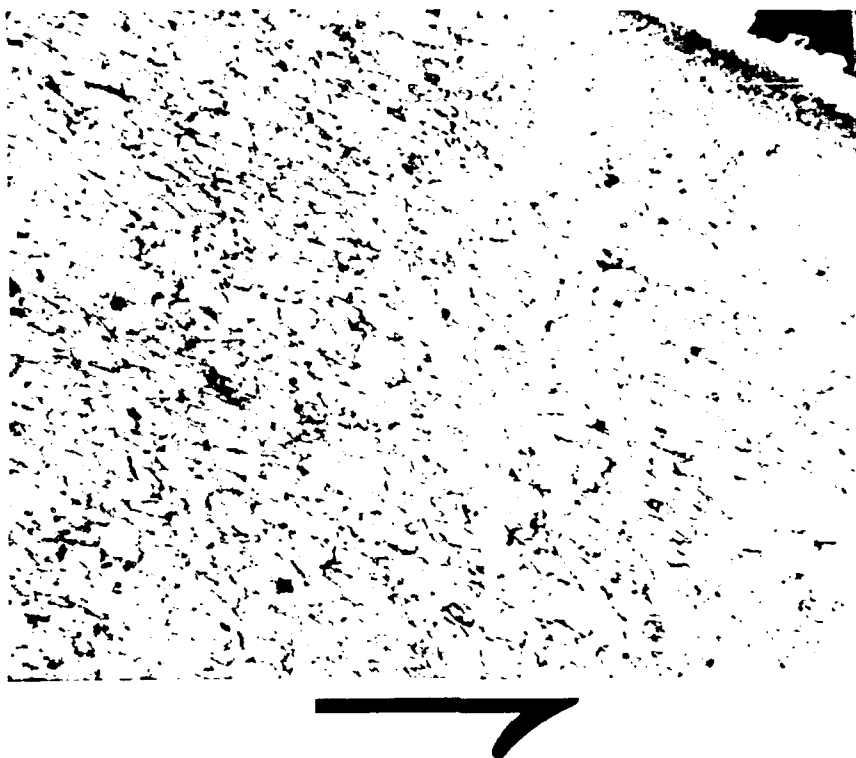Figure 16. Micrograph Along Edge of Penetration Channel (No. 2 in Figure 14).

Figure 17. Micrograph Inside Sheared Chip (No. 3 in Figure 14).

Arrow indicates
flight direction

1

2

3

4

5

INCHES
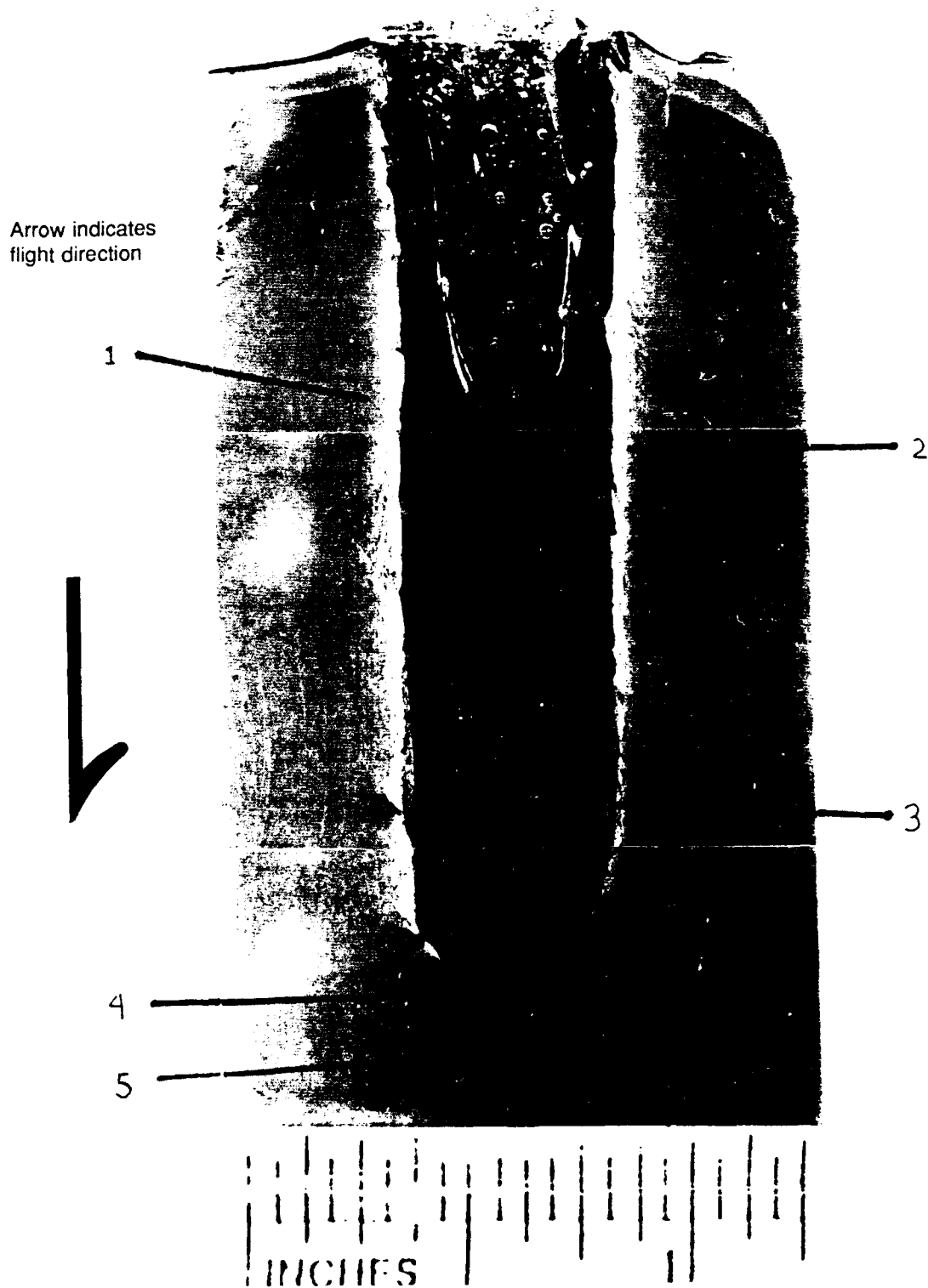
Figure 18. Enlarged View of RHA Target, Shot Number 4042.

Figure 19. Micrograph Along Edge of Penetration Channel (No. 1 in Figure 18).

Figure 20. Micrograph of Beginning of Shear Band (No. 2 in Figure 18).
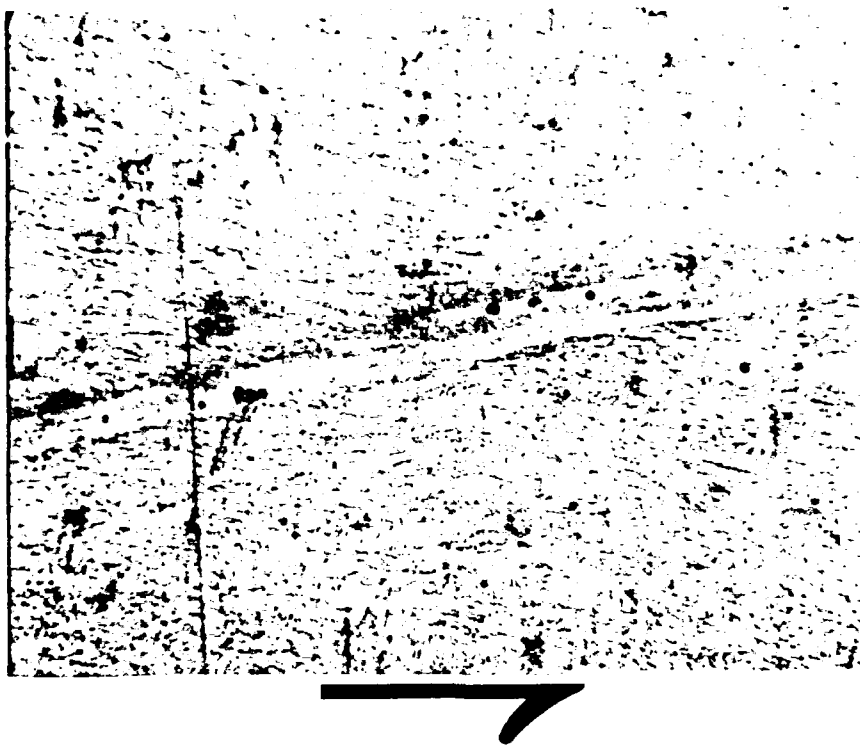
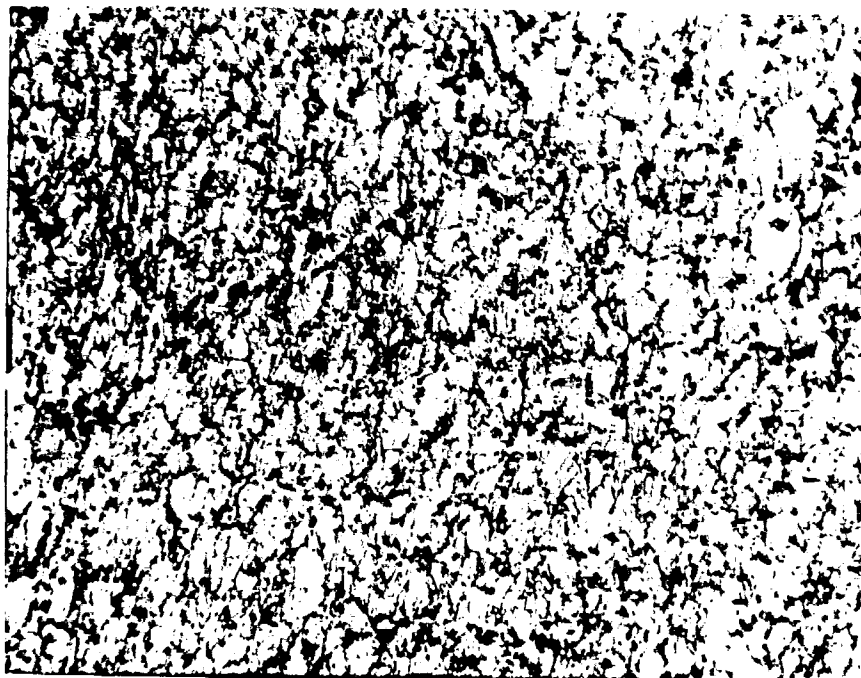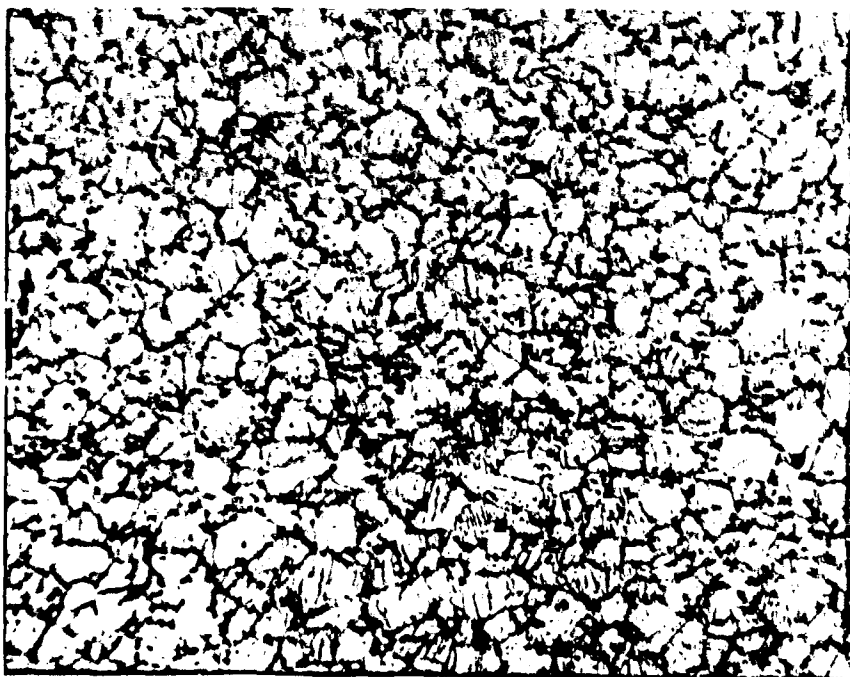Figure 21. Micrograph of Shear Band (No. 3 in Figure 18).
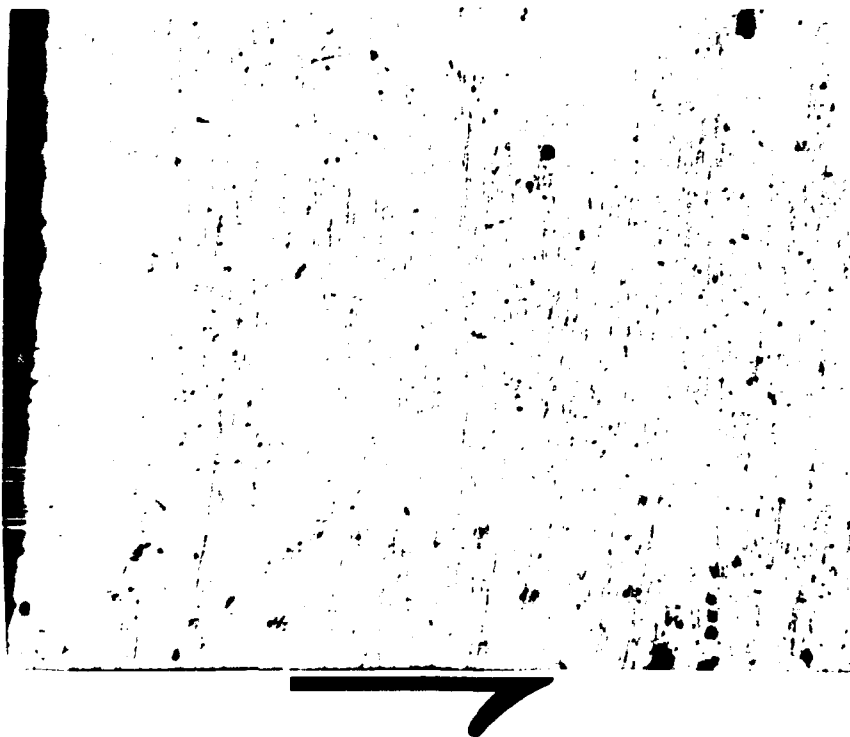
Figure 22. Micrograph Directly in Front of Penetration Channel (No. 4 in Figure 18).
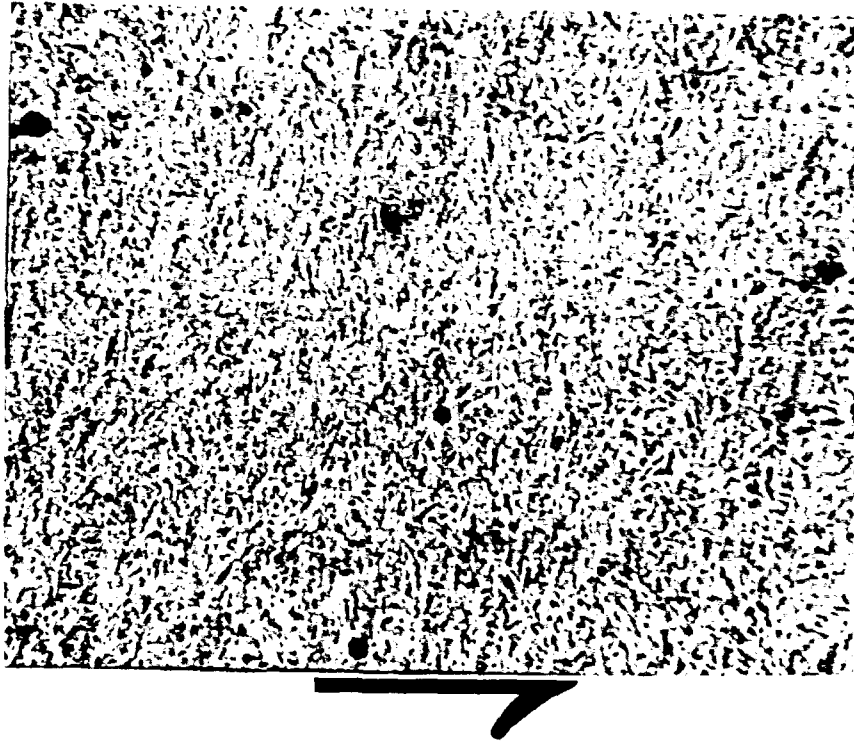
Figure 23. Micrograph Further in Front of Penetration Channel (No. 5 in Figure 18).

Arrow indicates
flight direction

Figure 24. Enlarged View of HHA Target, Shot Number 4043.

Figure 25. Micrograph of Virgin HHA Material (No. 1 in Figure 24).

Figure 26. Micrograph Directly in Front of Penetration Channel (No. 2 in Figure 24).
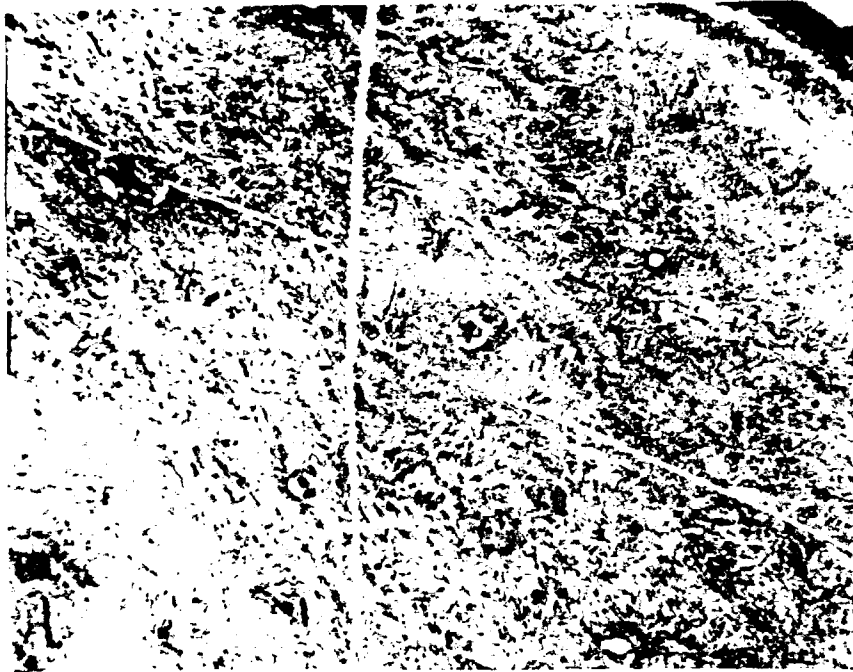
Figure 27. Micrograph Inside Sheared Chip (No. 3 in Figure 24).

Figure 28. Micrograph Inside Sheared Chip (No. 4 in Figure 24).

Arrow indicates
flight direction

3

1

2
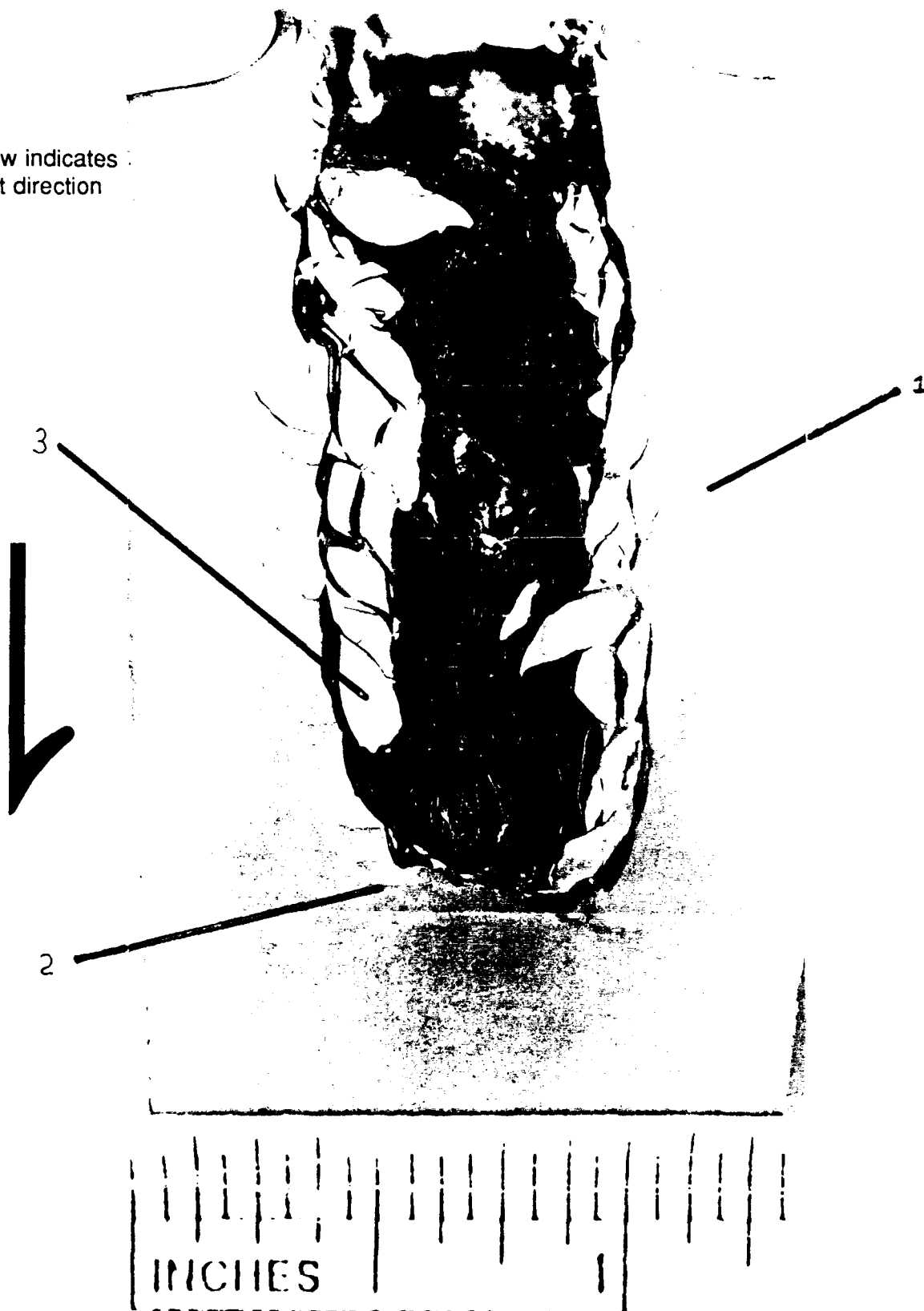
Figure 29. Enlarged View of HHA Target, Shot Number 4044.

INCHES
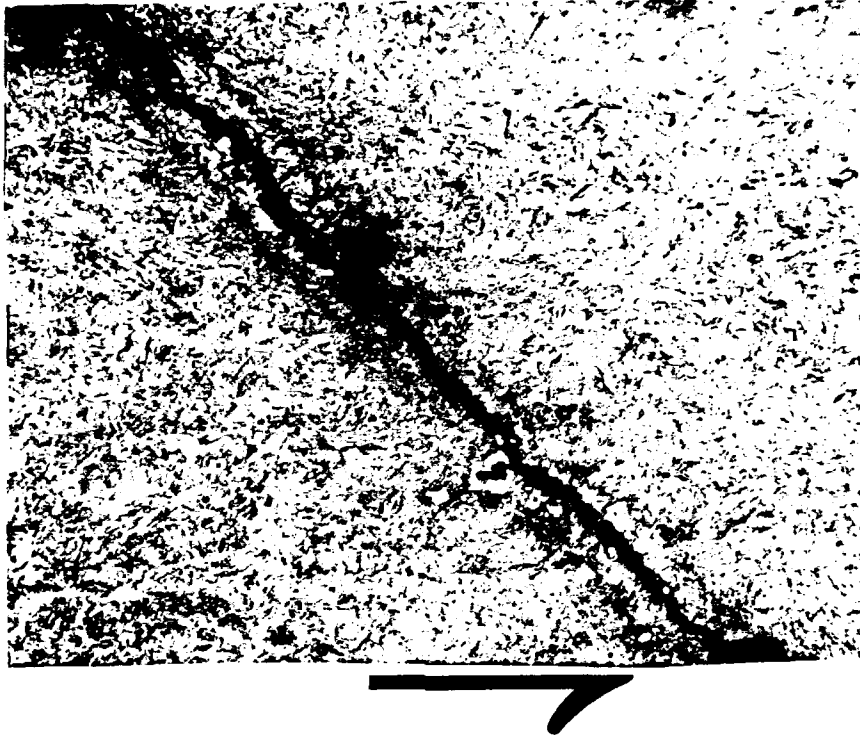
Figure 30. Micrograph Along Edge of Penetration Channel (No. 1 in Figure 29).
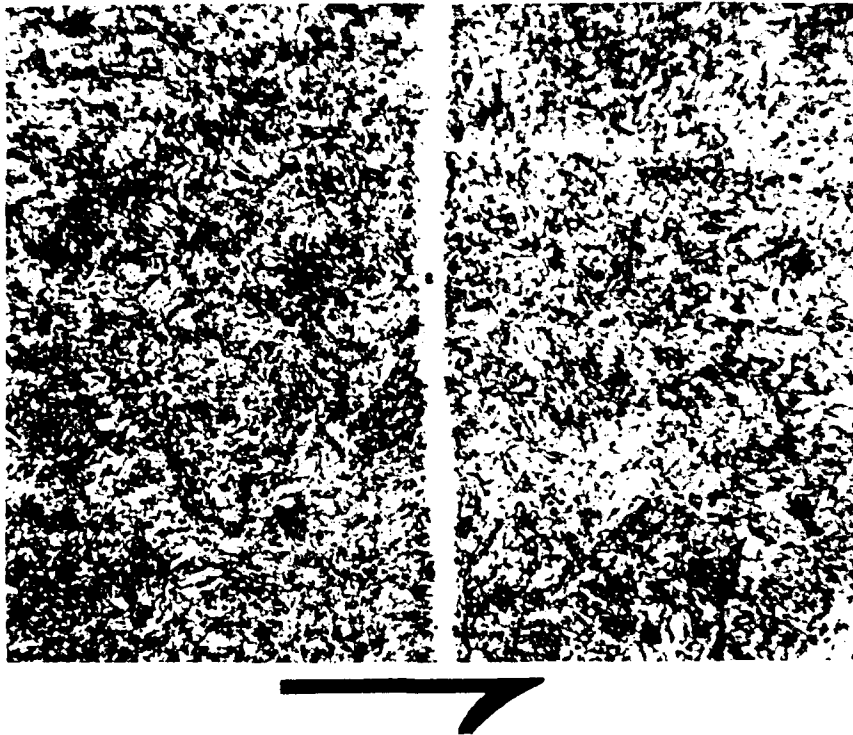
Figure 31. Micrograph Along Edge of Penetration Channel (No. 2 in Figure 29).

43

Figure 32. <u>Micrograph Inside Sheared Chip (No. 3 in Figure 29)</u>.

Arrow indicates
flight direction

Figure 33. Enlarged View of Pyromet 718 Target, Shot Number 4045.

45

Figure 34. Micrograph of Virgin Pyromet 718 Material (No. 1 in Figure 33).
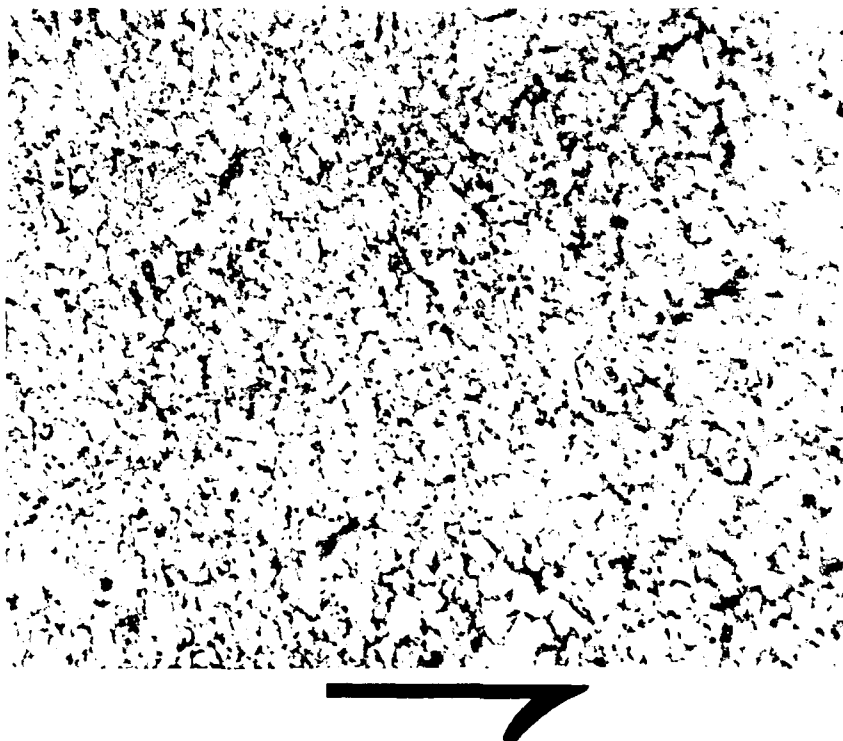
Figure 35. Micrograph in Front of Penetration Channel (No. 2 in Figure 33).

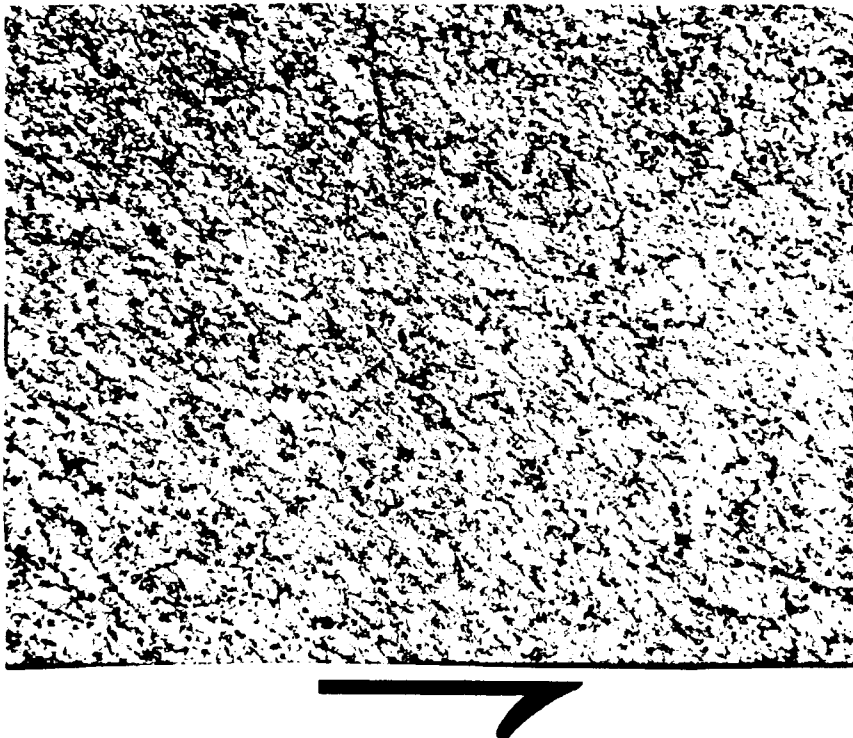Figure 36. <u>Micrograph</u> <u>ong Edge of Shear Chip (No. 3 in Figure 33)</u>.

Arrow indicates
flight direction
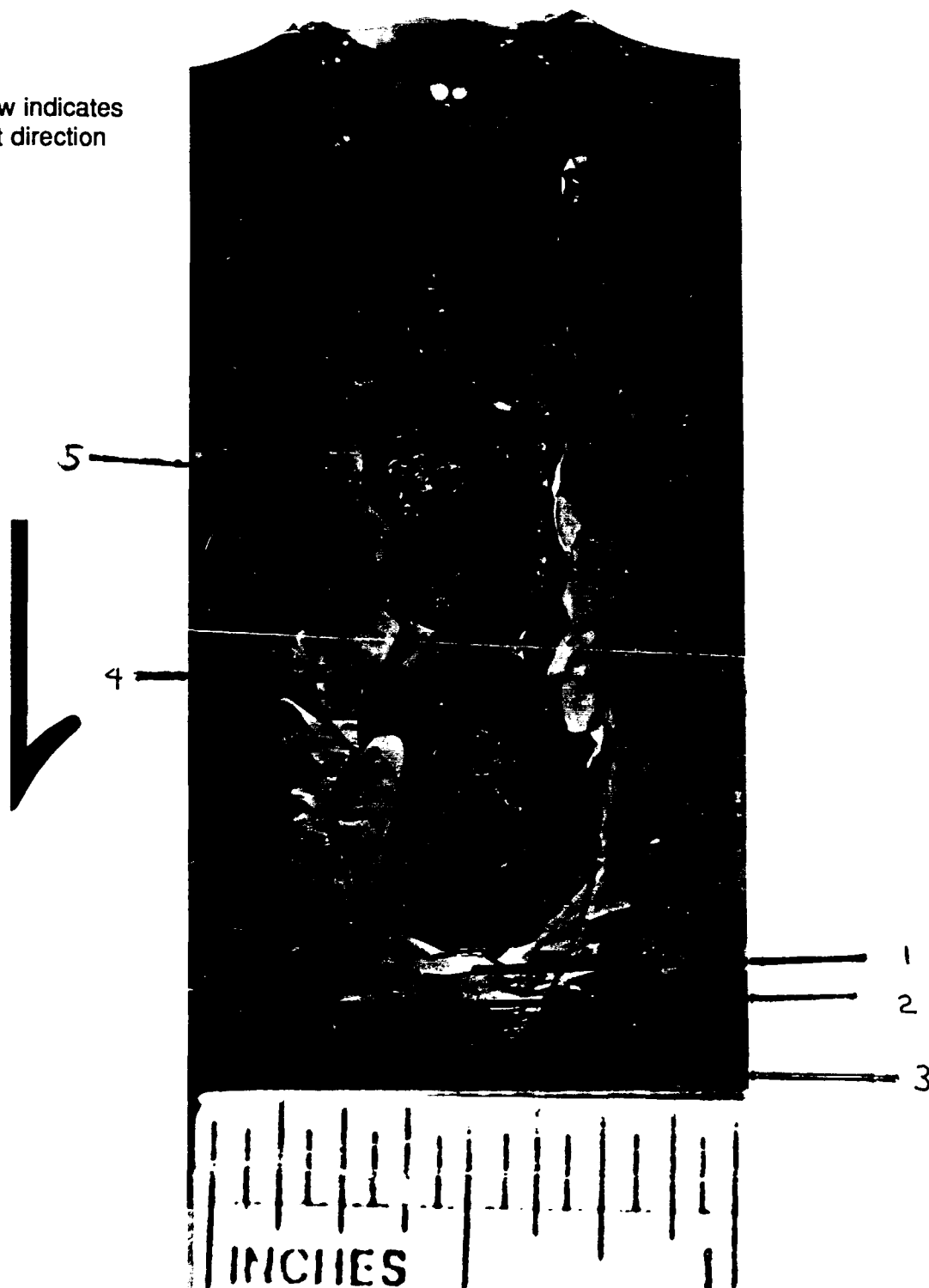
Figure 37. Enlarged View of Pyromet 718 Target, Shot Number 4047.

Figure 38. <u>Micrograph Directly in Front of Penetration Channel (No. 1 in Figure 37)</u>.

Figure 39. <u>Micrograph Somewhat in Front of Penetration Channel (No. 2 in Figure 37)</u>.

Figure 40. Micrograph Further in Front of Penetration Channel (No. 3 in Figure 37).
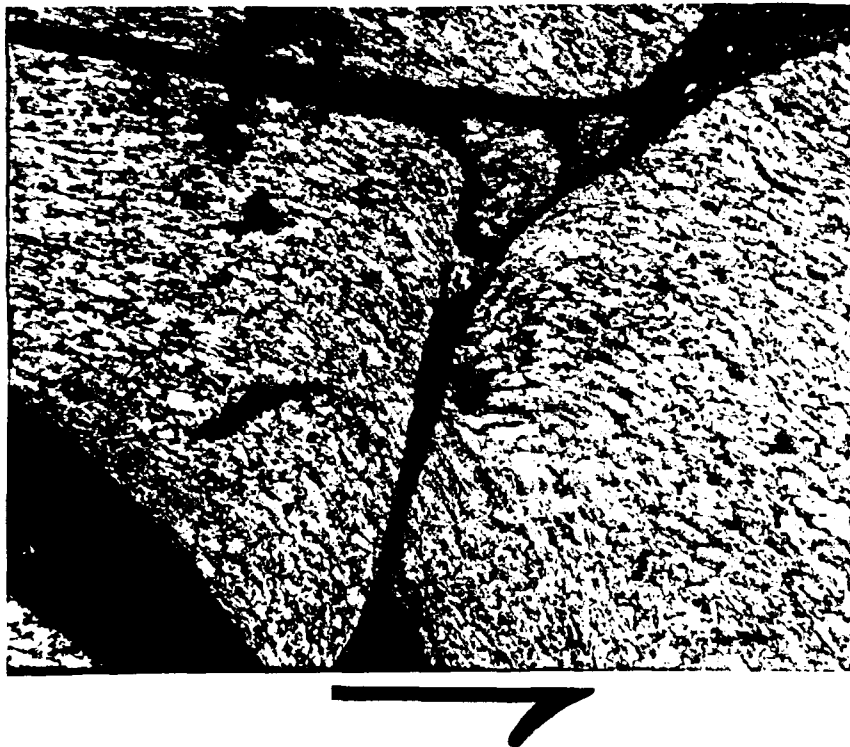
Figure 41. Micrograph of Interaction of Shear Chips (No. 4 in Figure 37).

Figure 42. Micrograph Inside Sheared Chip (No. 5 in Figure 37).

Arrow indicates
flight direction

1

2

2

3
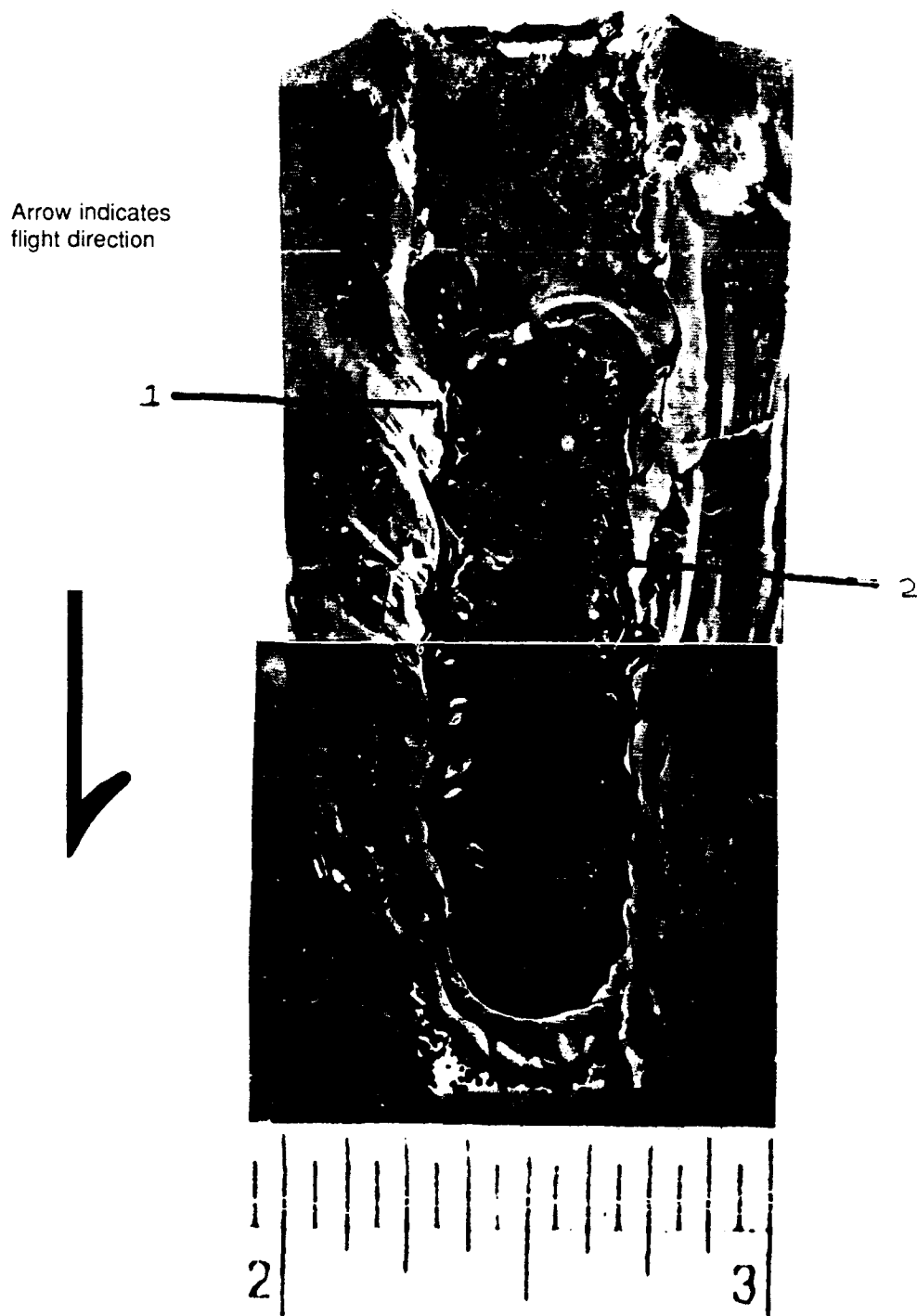
Figure 43. Enlarged View of Pyromet 718 Target, Shot Number 4046.
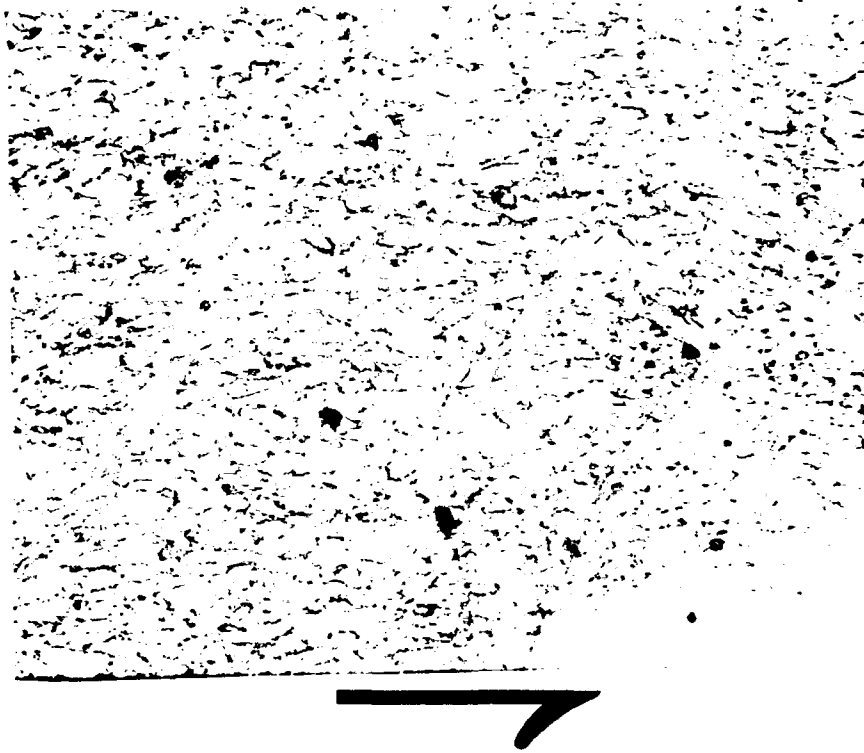
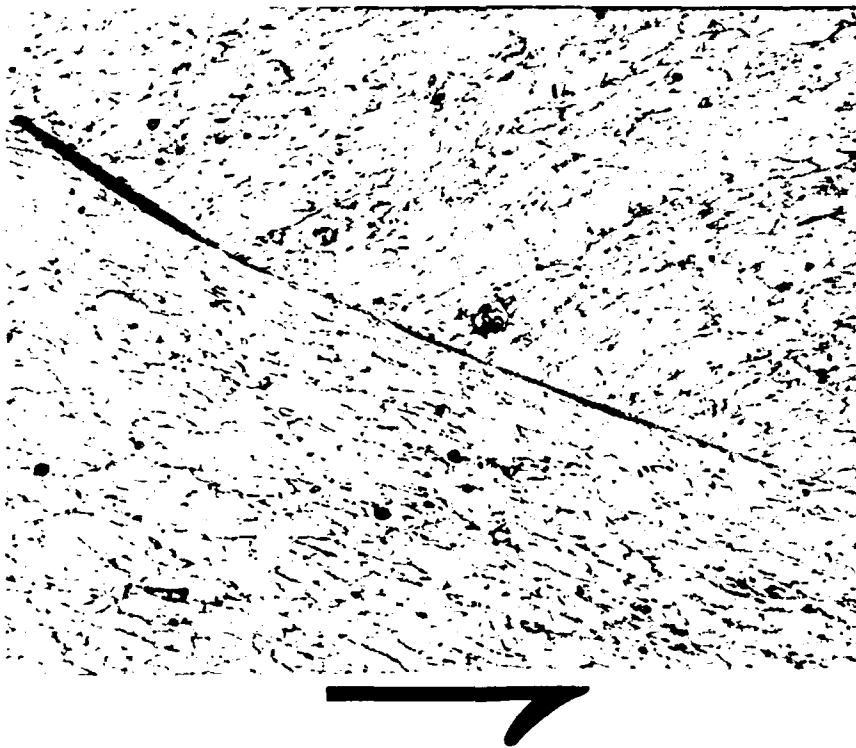Figure 44. Micrograph of Deformation Band (No. 1 in Figure 43).

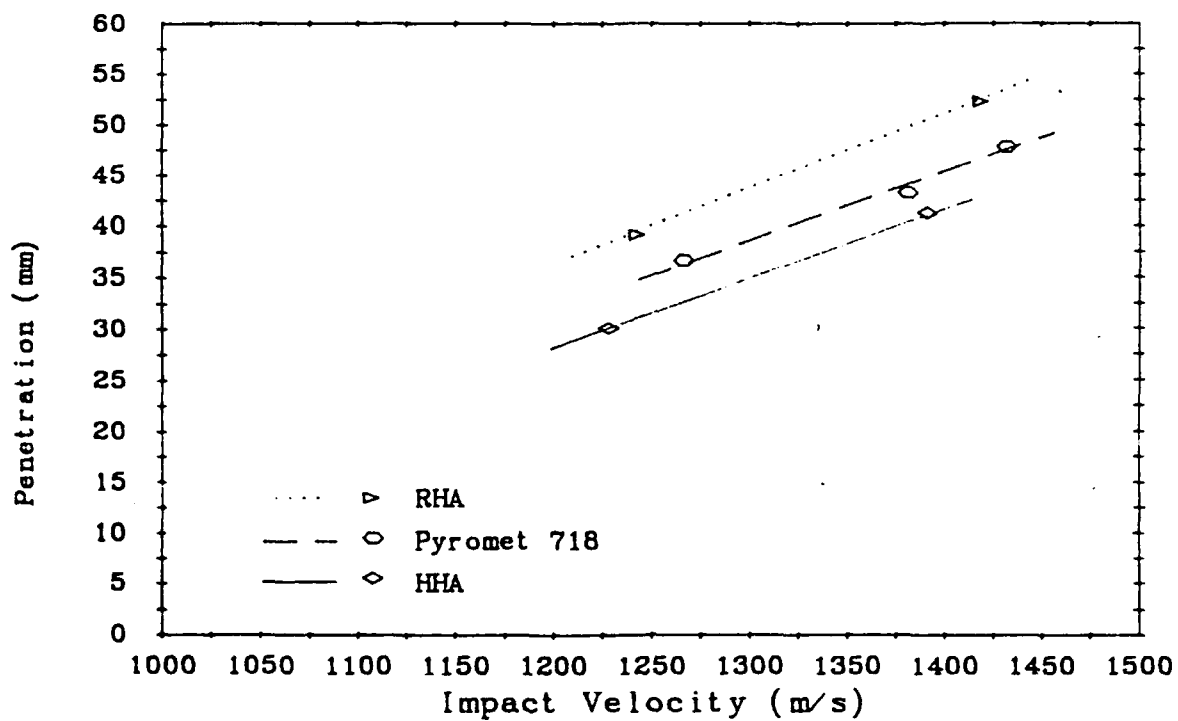Figure 45. Micrograph Along Edge of Chip (No. 2 in Figure 43).

Figure 46. Ballistic Plot of Impact Velocity vs. Depth of Penetration.
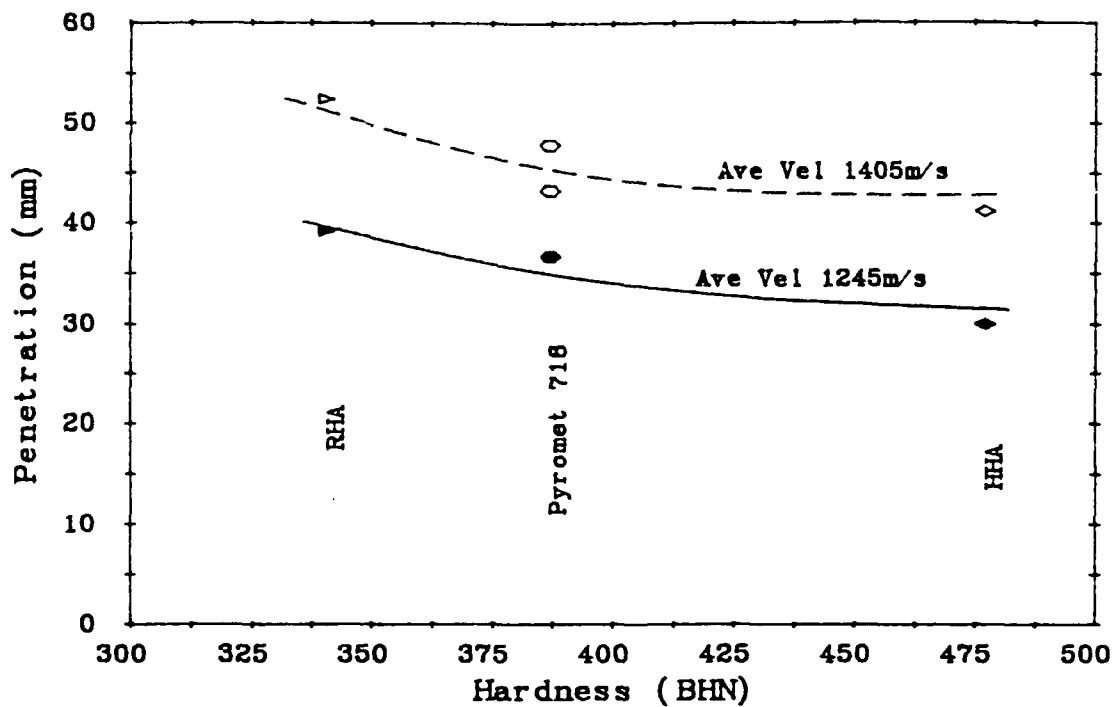

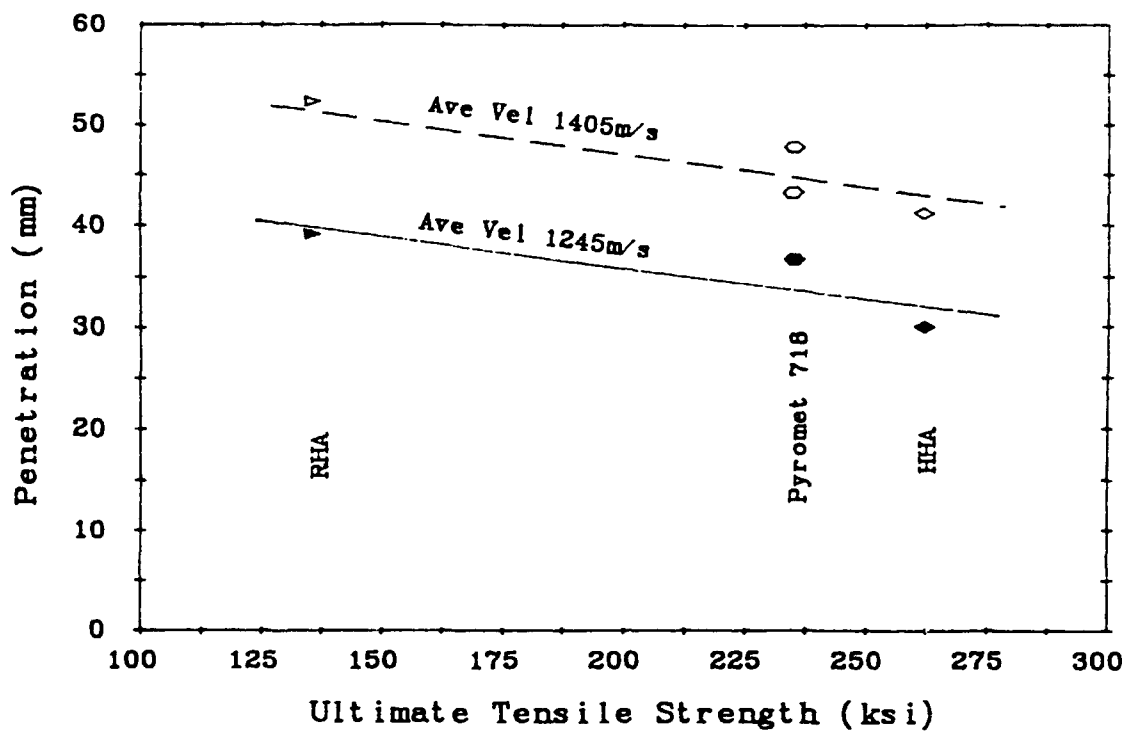Figure 47. Ballistic Plot of Depth of Penetration vs. Target Hardness (BHN).

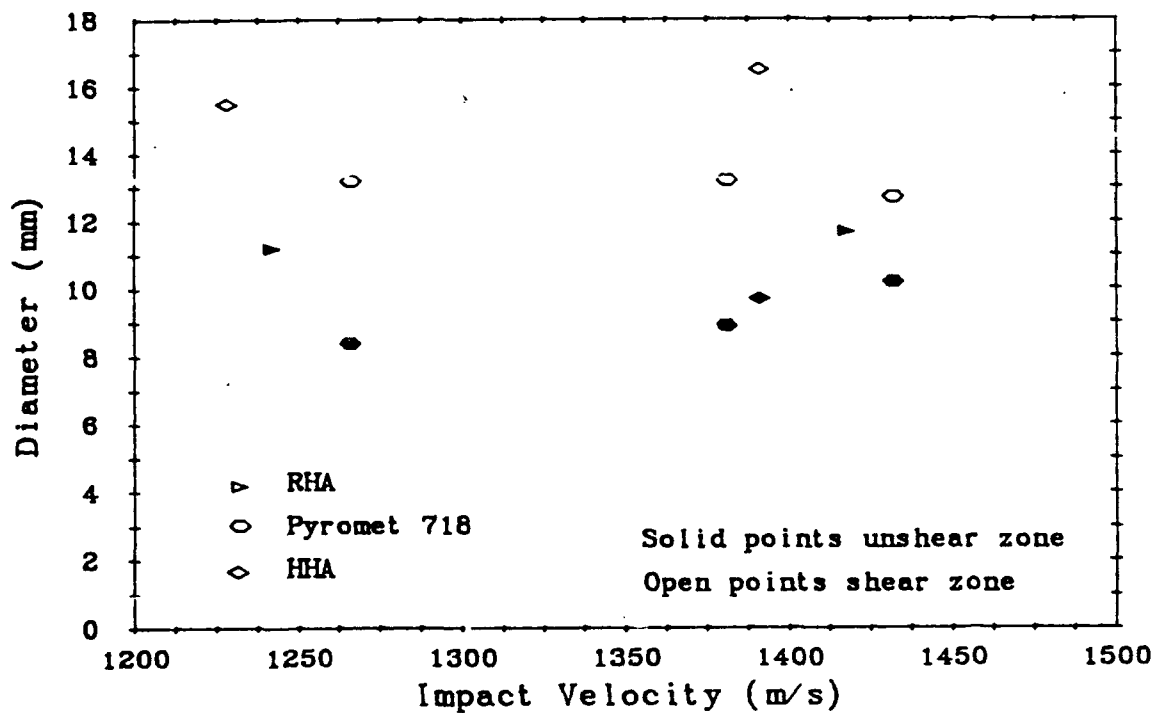Figure 48. Ballistic Plot of Depth of Penetration vs. Target Strength.

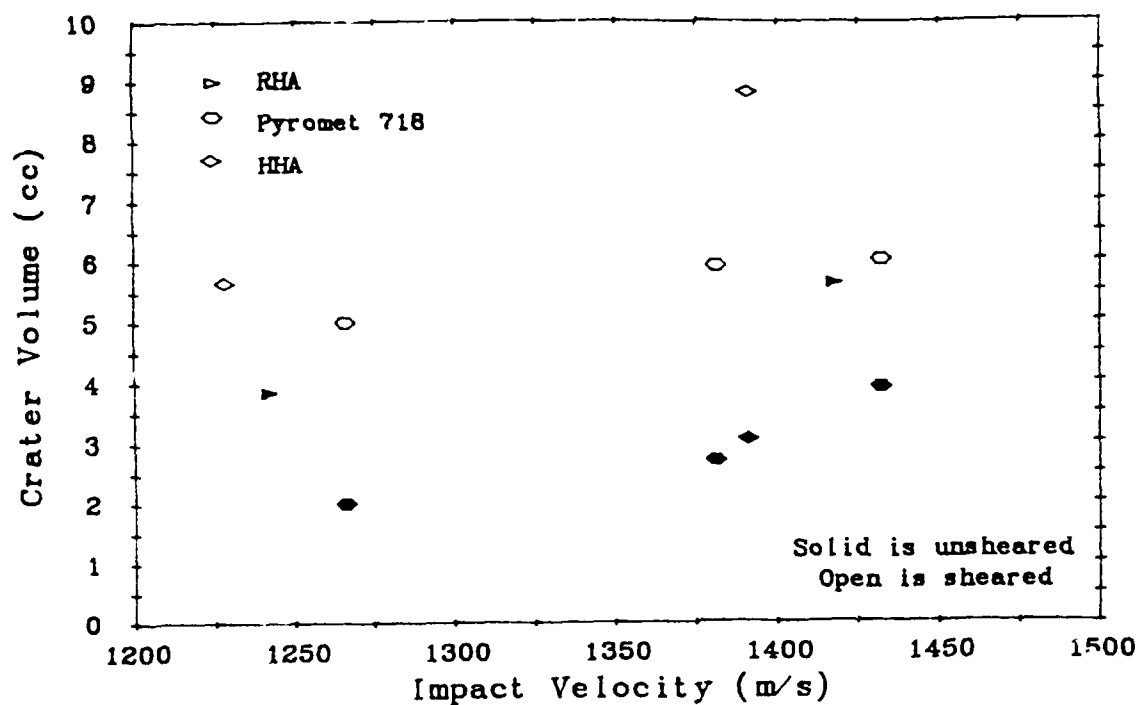Figure 49. Ballistic Plot of Impact Velocity vs. Channel Diameter.

55

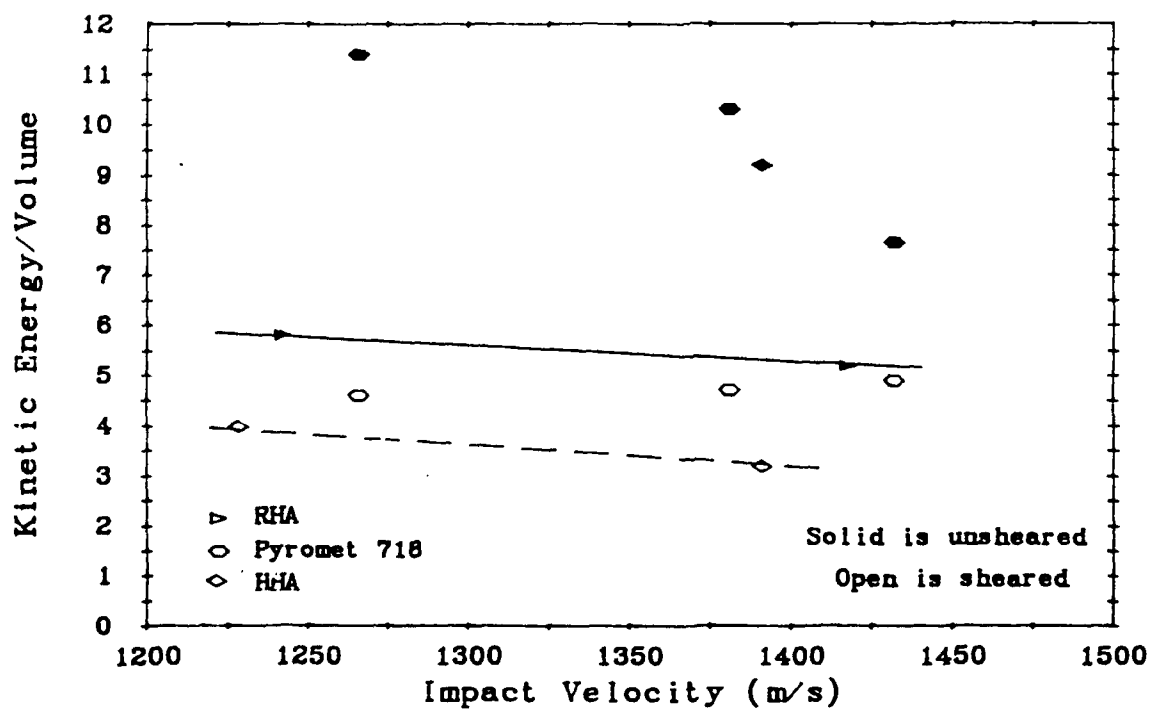Figure 50. Ballistic Plot of Impact Velocity vs. Channel Volume.

Figure 51. Ballistic Plot of Impact Velocity vs. Energy/Volume.

56

9. REFERENCES

Bjerke, T. W., G. F. Silsby, D. M. Scheffler, and R. M. Mudd. "Yawed Long Rod Armor Penetration at Ordnance and Higher Velocity." BRL-TR-3221, U.S. Army Ballistic Research Laboratory, Aberdeen Proving Ground, MD, March 1991.

Donachie, Matthew J., Compiler. Super Alloys Source Book. American Society of Metals, pg. 222, 1984.

Flockhart, C. J., R. L. Woodward, and R. G. O'Donnell. "Velocity Discontinuities and Shear Failure in Dynamic Plastic Deformation." The Technical Cooperation Program, Subgroup P- Materials Technology, Technical Panel 1 - Metallic Materials, January 1990.

Grabarek, C., and E. L. Herr. "X-Ray Multi-flash System for Measurement of Projectile Performance at the Target." Technical Note 1634, U.S. Army Ballistic Research Laboratory, Aberdeen Proving Ground, MD, September 1966.

Magness, L. S., and T. G. Farrand. "Deformation Behavior and its Relationship to the Penetration Performance of High-Density KE Penetrator Materials." Proceedings of Army Research Office Conference, October 1990.

Meyer, L. W., and F. J. Behler (Fraunhofer-Institute fur Angewandte Materialforshung, Bremen, W. Germany) and K. Frank and L. S. Magness (BRL). "Interdependence between the Dynamic Mechanical Properties and the Ballistic Behavior of Materials." Proceedings of 12th International Ballistic Symposium, San Antonio, TX, August 1990.

Meyers, M. A., and C. L. Wittman. "Effect of Metallurgical Parameters on Shear Band Formation in Low-Carbon (~.20 Wt Pct) Steels." Metalurgical Transactions, vol. 21A, pg. 3153–3164 December 1990.

Moss, G. L. "Shear Strains, Strain Rates and Temperature Changes in Adiabatic Shear Bands." BRL-TR-02242, U.S. Army Ballistic Research Laboratory, Aberdeen Proving Ground, MD, May 1980.

Staker, M. R. "The Relation Between Adiabatic Shear Instability Strain and Material Properties." Acta Metallurgica, vol. 29, pg. 683–689, 1981.

Woodward, R. L, B. J. Baxter, and N. V. Y. Scarlett. "Mechanisms of Adiabatic Shear Plugging in High Strength Aluminum and Titanium Alloys." The Institute of Physics Conference, Ser. No. 70, Oxford, 1984.

Yellup, J. M., and R. L. Woodward. "Investigations Into the Prevention of Adiabatic Shear Failure in High Strength Armour Materials." Res Mechanica 1, pg. 41–57, 1980.

Zener, C., and J. H. Holloman. "Effect of Strain Rate Upon Plastic Flow of Steel." Journal of Applied Physics, vol. 15, pg. 22–32, 1944.

INTENTIONALLY LEFT BLANK.

USER EVALUATION SHEET/CHANGE OF ADDRESS

This laboratory undertakes a continuing effort to improve the quality of the reports it publishes. Your comments/answers below will aid us in our efforts.

1. Does this report satisfy a need? (Comment on purpose, related project, or other area of interest for which the report will be used.) _____

_____

2. How, specifically, is the report being used? (Information source, design data, procedure, source of ideas, etc.) _____

_____

3. Has the information in this report led to any quantitative savings as far as man-hours or dollars saved, operating costs avoided, or efficiencies achieved, etc? If so, please elaborate. _____

_____

4. General Comments. What do you think should be changed to improve future reports? (Indicate changes to organization, technical content, format, etc.) _____

_____

BRL Report Number ___BRL–TR–3255___   Division Symbol _____

Check here if desire to be removed from distribution list. ____

Check here for address change. ____

Current address: Organization _____
                     Address   _____
                                   _____